ฟลูออเรสเซนต์เซ็นเซอร์แบบเปิดจากเกลืออินโดเลียมสำหรับการตรวจวัดไซยาไนด์

นายอภิวัฒน์ พรหมชาติ

วิทยานิพนธ์นี้เป็นส่วนหนึ่งของการศึกษาตามหลักสูตรปริญญาวิทยาศาสตรมหาบัณฑิต
สาขาวิชาเคมี ภาควิชาเคมี
คณะวิทยาศาสตร์ จุฬาลงกรณ์มหาวิทยาลัย
ปีการศึกษา 2558

TURN-ON FLUORESCENT SENSORS FROM INDOLIUM SALT FOR CYANIDE DETECTION

Mr. Apiwat Promchat

A Thesis Submitted in Partial Fulfillment of the Requirements
for the Degree of Master of Science Program in Chemistry
Department of Chemistry
Faculty of Science
Chulalongkorn University
Academic Year 2015

Thesis Title	TURN-ON FLUORESCENT SENSORS FROM INDOLIUM SALT FOR CYANIDE DETECTION
By	Mr. Apiwat Promchat
Field of Study	Chemistry
Thesis Advisor	Professor Mongkol Sukwattanasinitt, Ph.D.
Thesis Co-Advisor	Associate Professor Paitoon Rashatasakhon, Ph.D.

Accepted by the Faculty of Science, Chulalongkorn University in Partial Fulfillment of the Requirements for the Master's Degree

.....Dean of the Faculty of Science
(Associate Professor Polkit Sangvanich, Ph.D.)

THESIS COMMITTEE

.....Chairman
(Associate Professor Vudhichai Parasuk, Ph.D.)

.....Thesis Advisor
(Professor Mongkol Sukwattanasinitt, Ph.D.)

.....Thesis Co-Advisor
(Associate Professor Paitoon Rashatasakhon, Ph.D.)

.....Examiner
(Professor Orawon Chailapakul, Ph.D.)

.....External Examiner
(Nakorn Niamnont, Ph.D.)

อภิวัฒน์ พรหมชาติ : ฟลูออเรสเซนต์เซ็นเซอร์แบบเปิดจากเกลืออินโดเลียมสำหรับการตรวจวัดไซยาไนด์ (TURN-ON FLUORESCENT SENSORS FROM INDOLIUM SALT FOR CYANIDE DETECTION) อ.ที่ปรึกษาวิทยานิพนธ์หลัก: ศ. ดร.มงคล สุขวัฒนาสินิทธิ์, อ.ที่ปรึกษาวิทยานิพนธ์ร่วม: รศ. ดร.ไพฑูรย์ รัชตะสาคร, 66 หน้า.

ตัวรับรู้เรืองแสงแบบเปิดสัญญาณฟลูออเรสเซนต์ที่มีความจำเพาะเจาะจงต่อไซยาไนด์ได้พัฒนาขึ้นจากเบนซิลลิดีนที่มีหมู่เมทิลอินโดเลียม โดยอนุพันธ์ของเบนซิลลิดีนสามชนิดถูกสังเคราะห์ได้จากปฏิกิริยาการควบแน่นระหว่างเบนซัลดีไฮด์สามชนิดกับเมทิลอินโดลีน มีเพียงเบนซิลลิดีนที่มีระบบคอนจูเกชั่นยาวที่สุดให้สัญญาณการเรืองแสงสีฟ้าอย่างจำเพาะเจาะจงต่อไซยาไนด์ และสามารถสังเกตได้ด้วยตาเปล่าในช่วงความเข้มข้นต่ำกว่าระดับไมโครโมลาร์ซึ่งเป็นผลเนื่องจากปฏิกิริยาการเติมของไซยาไนด์ที่หมู่อินโดเลียม การตรวจวัดไซยาไนด์ด้วยสารนี้ได้ถูกปรับปรุงให้สามารถตรวจวัดในตัวกลางที่เป็นน้ำโดยใช้สารลดแรงตึงผิวชนิดไม่มีขั้ว และใช้วิธีโซนิเคชั่นเพื่อให้ได้ค่าการตรวจวัดที่ต่ำที่สุดในช่วงต่ำกว่านาโนโมลาร์โดยไม่ใช้ตัวทำละลายอินทรีย์ในระบบการตรวจวัด อีกทั้งยังได้พัฒนาการตรวจวัดโดยใช้กระดาษและเจลเพื่อให้สามารถใช้ตรวจวัดนอกสถานที่ด้วยตาเปล่าที่ความเข้มข้นระดับไมโครโมลาร์ภายใต้แสงยูวีชนิดคลื่นยาว (360 นาโนเมตร)

ภาควิชา เคมี	ลายมือชื่อนิสิต .....
สาขาวิชา เคมี	ลายมือชื่อ อ.ที่ปรึกษาหลัก .....
ปีการศึกษา 2558	ลายมือชื่อ อ.ที่ปรึกษาร่วม .....

5672138823 : MAJOR CHEMISTRY

KEYWORDS: CYANIDE SENSOR / FLUORESCENT SENSOR / INDOLIUM / BENZYLIDENES

APIWAT PROMCHAT: TURN-ON FLUORESCENT SENSORS FROM INDOLIUM SALT FOR CYANIDE DETECTION. ADVISOR: PROF. MONGKOL SUKWATTANASINITT, Ph.D., CO-ADVISOR: ASSOC. PROF. PAITOON RASHATASAKHON, Ph.D., 66 pp.

A highly sensitive turn-on fluorescent sensor for cyanide was developed based on benzylidenes containing methylindolium group. Three benzylidene derivatives were synthesized from the condensations of three benzaldehyde derivatives and methyleneindoline. Only the longest conjugated system of these three derivatives showed strong blue fluorescent response selectively to CN^- which was clearly observed in submicromolar range as the result of the cyanide addition to the indolium group. The detection of cyanide with this compound was optimized in aqueous media using nonionic surfactant and sonication method to give very low limit of detection in subnanomolar range which nonorganic solvent in sensing system. The compound is also developed into a paper-based and gel-based sensing kits for on–site naked eye detection of cyanide in micromolar range under a common black light (360 nm) illumination.

Department:	Chemistry	Student's Signature	.....
Field of Study:	Chemistry	Advisor's Signature	.....
Academic Year:	2015	Co-Advisor's Signature	.....

ACKNOWLEDGEMENTS

I wish to express my sincere gratitude to my advisor, Professor Mongkol Sukwattanasinitt, Ph.D., my co-advisor Associate Professor Paitoon Rashatasakhon, Ph.D., Assistant Professor Anawat Ajavakom, Ph.D., Assistant Professor Sumrit Wacharasindhu, Ph.D., and Sakulsuk Unarunotai, Ph.D. for their generous guidance, excellent and kind supervision, and helpful suggestion throughout this research. This thesis research would not be completed without their advice and support.

My appreciation is also given to Associate Professor Vudhichai Parasuk, Ph.D., and Professor Orawan chailapakul, Ph.D. thesis defense committee, for their kind attention, beneficial suggestion and recommendations. I would like to thank Nakorn Niamnont, Ph.D., thesis defense committee from King Mongkut's University of Technology Thonburi for advices. I would like to express my gratitude to Department of chemistry, Faculty of Science, Chulalongkorn University for providing the chemicals and facilities throughout the course of study.

Furthermore, I appreciatively thank to my friends, Miss Kanokthorn, Mr. Jadetaphong, Miss Atchareeporn, Mr. Chakrit and everyone in Material Advancement via Proficient Synthesis (MAPS group) for their honesty, spirit, good wish and help during the course of my graduate research.

This study is financially supported by Nanotechnology Center (NANOTEC), NSTDA, Ministry of Science and Technology, Thailand, through its program of Center of Excellence Network and Science Achievement Scholarship of Thailand (SAST). This work is part of the Project for Establishment of Comprehensive Center for Innovative Food, Health Products and Agriculture supported by the Thai Government Stimulus Package 2 (TKK2555, SP2) and the Ratchadaphiseksomphot Endowment Fund of Chulalongkorn University (RES560530126-AM).

Finally, I would like to express my gratitude to my parents who always stand by my side during both of my plesent and hard time.

CONTENTS

Page

Page

Page

LIST OF TABLES

LIST OF FIGURES

LIST OF SCHEME

LIST OF ABBREVIATIONS

A	acceptor
calcd.	calculated
^{13}C NMR	carbon-13 nuclear magnetic resonance
$CDCl_3$	deuterated chloroform
CHES	2-(Cyclohexylamino)ethanesulfonic acid
cm	centimeter
D	donor
d	doublet (NMR)
dd	doublet of doublet (NMR)
DMF	N,N'-dimethyl formamide
equiv.	equivalent (s)
EtOAc	ethyl acetate
g	gram (s)
h	hour (s)
^{1}H-NMR	proton nuclear magnetic resonance
HRMS	high resolution mass spectroscopy
Hz	hertz
ICT	intramolecular charged transfer
J	coupling constant
m	multiplet (NMR)
M	molar
Me	methyl

MHz	megahertz
mg	milligram (s)
min	minute (s)
mL	milliliter (s)
mmol	millimole (s)
m/z	mass per charge
nm	nanometer
nM	nanomolar
OAc	acetate
OMe	methoxy
pg	pico gram (s)
ppm	part per million
rt	room temperature
s	singlet (NMR)
t	triplet (NMR)
THF	tetrahydrofuran
UV	ultraviolet
δ	chemical shift
°C	degree Celsius
µL	microliter (s)
µM	micromolar (s)
Φ	quantum yield
% yield	percentage yield

CHAPTER I

INTRODUCTION

1.1 Photophysical processes for fluorescence

At normal temperature, an organic molecule is in its ground electronic state called S_0 which is a singlet state. The molecule can temporary assume one of the higher energy electronic states called excited state when it absorbs a photon of light with suitable energy. The electronic transition due to light absorption is extremely fast (10^{-16}-10^{-14} s) that the absorption of two photons or multiple photons to give a single electronic transition does not generally occur, except under an extreme intensity of light such as a cross of two laser beams. The transition from one electronic state to another must also obey certain restrictions. In particular, high probability transitions must be spin conservative. Thus, S_0 will be excited to one of the higher singlet states such as S_1 or S_2 (**Figure 1.1**).

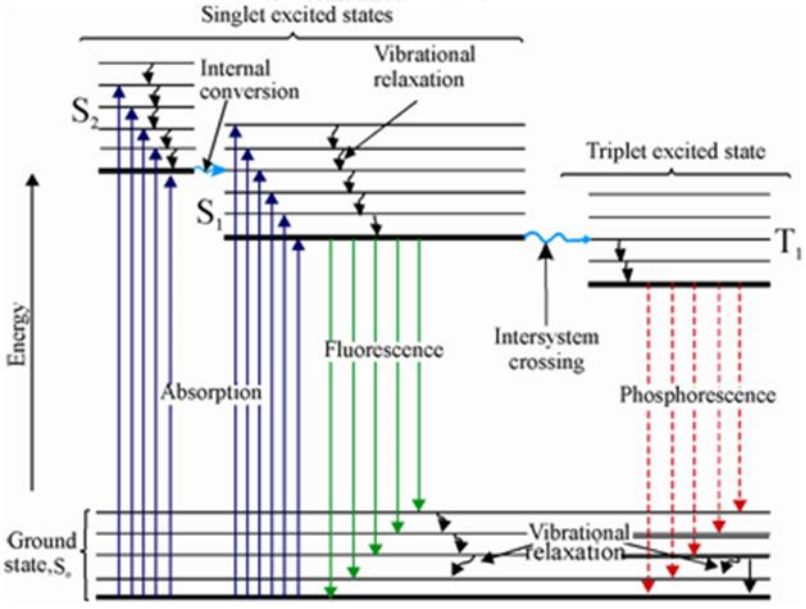

Figure 1.1 Jablonski diagram describing photophysical processes [1].

As the mass of a nucleus is much higher than the mass of an electron, the nuclear motions are much slower than the electron motions which is the basis of Franck-Condon principle. Therefore, the electronic transition occurs without geometry change which is often called vertical transition. If the appropriate geometry of the

excited state is different from the ground state, the initial electronic excitation will produce an unfavorable geometry of the excited state which will geometrically relaxed to the most stable vibrational state of S_1 via vibration and rotation without emitting light. This nonradiative decay normally happens within 10^{-11} s or less. If the initial excited state is higher than S_1, the molecule may relax to the most stable vibrational state of S_1 via the coupling of geometrical and electronic relaxation which is termed as internal conversion.

At the most stable vibrational state of S_1, the molecule can return to S_0 by two radiative pathways. First, the direct relaxation from S_1 back to S_0 which is referred to fluorescence which usually takes 10^{-8}-10^{-5} s. With part of the energy nonradiatively lost via geometrical relaxation and internal conversion, fluorescence spectrum is typically observed at longer wavelength than absorption spectrum. The wavelength difference between absorption and emission peaks is called Strokes shift. The molecules with many possible geometry changes will have larger Stokes shift. However, in rigid molecules for which S_1 and S_0 have very similar geometries, and the solvation, the Stokes shift will be small. The second pathway that can exit S_1 state is an inter system crossing (ISC) which converts electron spin from singlet to triplet state (T_1). Usually, the transitions between S_1 to T_1 in common organic molecule are forbidden by the spin conservation rule. However, a molecule containing heavy atoms like bromine or iodine can couple angular momentum change with the spin conversion and the ISC is allowed. After ISC process, radiative relaxation from T_1 back to S_0 is known as phosphorescence. The rates of phosphorescence are around 10^2-10 s^{-1} that phosphorescence has very long lifetimes in the range of seconds to minutes. A phosphorescent sample can continue to glow even after the excitation source is turned off.

1.2 Fluorescence quenching

Fluorescence quenching can be divided into two major mechanisms, first is dynamic quenching which is controlled by the diffusion rate of the fluorophore and quencher. As shown in Figure 1.2A, dynamic quenching appears when the excited state

fluorophore (F*) is deactivated upon interact with quencher (Q) and return to S_0 without emitted photon. Second is static quenching (Figure 1.2B) which is a result of stable non-fluorescent complex (F·Q) between the fluorophore (F) and the quencher. This complex absorbs the excitation light and returns to the ground state via various nonradiative mechanisms without emitting fluorescence. The static quenching efficiency is related to the association constant (K_a) for F·Q complexation [2].

There are several methods to characterize these two mechanisms. First, fluorescence lifetime decay in dynamic quenching decreases in ratio to the intensity, however it does not change in static quenching, because the fluorescence occurs from the non-complexed fluorophore, which remains the same. Second way is to compare the quenching efficiency at various temperature. The static quenching efficiency decreases with increasing temperature as a result of the weakening of the binding, while dynamic quenching efficiency increases with increasing temperature due to faster diffusion and collision.

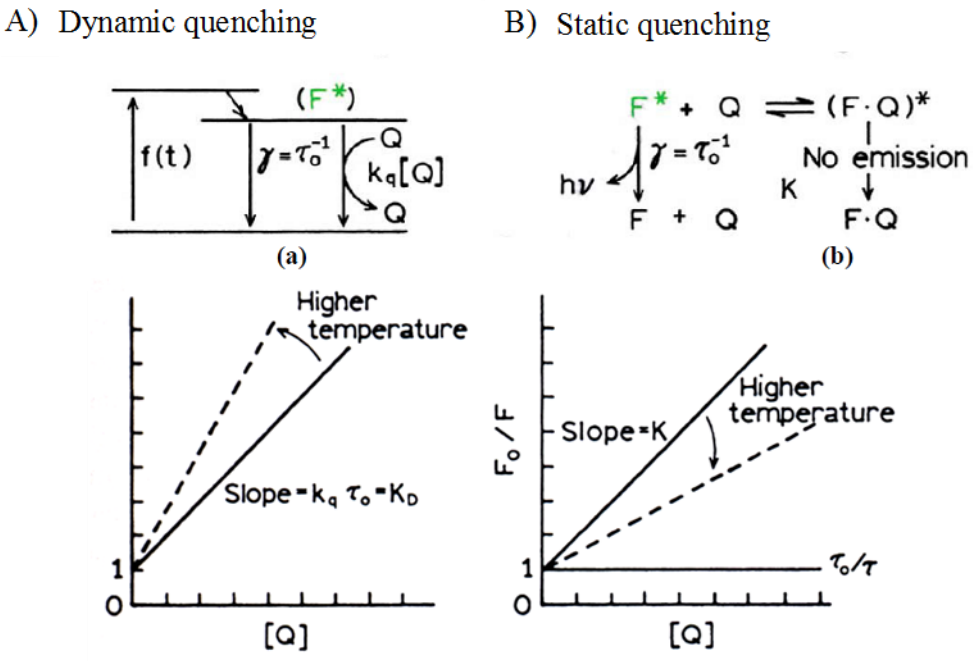

Figure 1.2 Mechanism of fluorescence quenching. A) Dynamic quenching. B) Static quenching [3].

1.3 Fluorescence sensors

Recently, selective sensors have been developed for simple to use and fast detection of various analytes. Fluorescent chemosensors generally offer several attractive features such as high sensitivity, satisfying selectivity, visual detection and optical imaging.

1.3.1 Sensing modes

A normal fluorescent chemosensor contains the recognition site (receptor) which has high affinity with the intended target linked to the signal source (fluorophore) which turns the detection result into the fluorescence signal. Also, the ideal fluorophore should not be affected by environmental interference (signal-selectivity), such as photochemical reactions, concentration and matrixes (pH, polarity, temperature, etc.). Fluorescent sensors may be classified into three types according to the response modes: turn-on, turn-off and wavelength shift. Turn-on mode is fluorescent sensor that give enhanced fluorescence signal upon interaction with an analyte. (Figure 1.3a) On the other hand, Turn-off mode must have fluorophore unit which is high emission intensity and give lower emission intensity upon interaction with an analyte. (Figure 1.3b) Wavelength shift is a mode that sensor molecule change the geometry when interaction with analyte then give a new fluorescence signal at different wavelength. (Figure 1.3c)

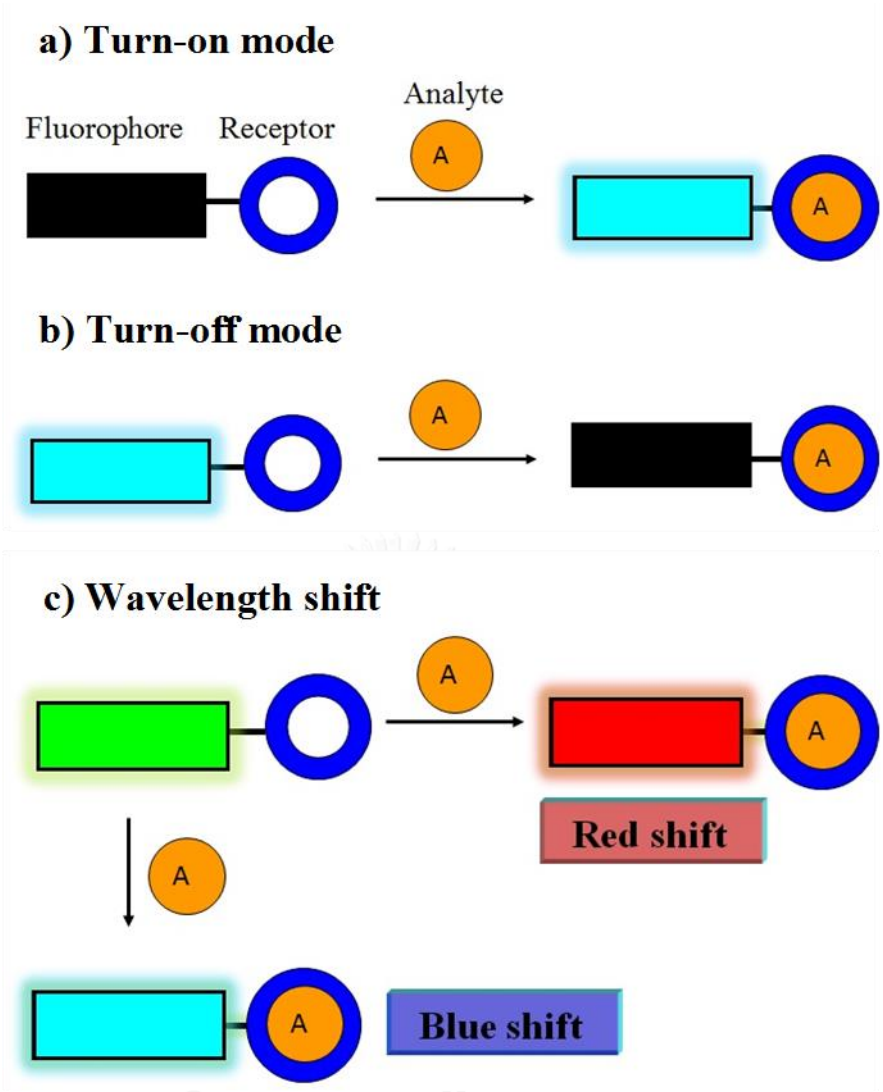

Figure 1.3 Modes of fluorescence responses.

1.3.2 Sensing mechanisms

The changes of fluorescence signals of the fluorescent sensors upon the interaction with analytes have been explained by theories involving the following photophysical processes: a) FÖrster resonance energy transfer (FRET), b) photoinduced electron transfer (PET), c) intramolecular charge transfer (ICT) and d) excited-state intramolecular proton transfer (ESIPT). A chemosensor may transduce the interaction event into fluorescent signals based on one or more of these processes. A design of sensing system having more than one processes working synergistically to enhance the fluorescence responses are challenging and required good understanding of the system.

a. FRET

The FÖrster resonance energy transfer (FRET) between two molecules is an important photophysical phenomenon applied in studying biological systems and biomedical research. FRET occurs when the emission spectrum of a donor fluorophore (D) overlaps with the absorption spectrum of acceptor fluorophore (A) (Figure 1.4). FRET is not the result of emission from the donor being absorbed by the acceptor. There is no intermediate photon in FRET. The mechanism is D in an excited electronic state, which transfer its excitation energy to a nearby A in nonradiative decay through long range dipole-dipole interactions. The supporting theory is based on the idea of an oscillating dipole that can undergo an energy exchange with a second dipole which has a similar resonance frequency. Also, resonance energy transfer is similar behavior of coupled oscillators. FRET is highly distance dependent, it is thus one of few tools available as "spectroscopic ruler" for measuring nanometer scale distances and the changes in distances, both in vitro and in vivo, such as measurements of distance between active sites on a protein that has been labelled with donor-acceptor fluorophores. Also, a turn off fluorescent sensor or a shift of wavelength can be designed based on FRET process.

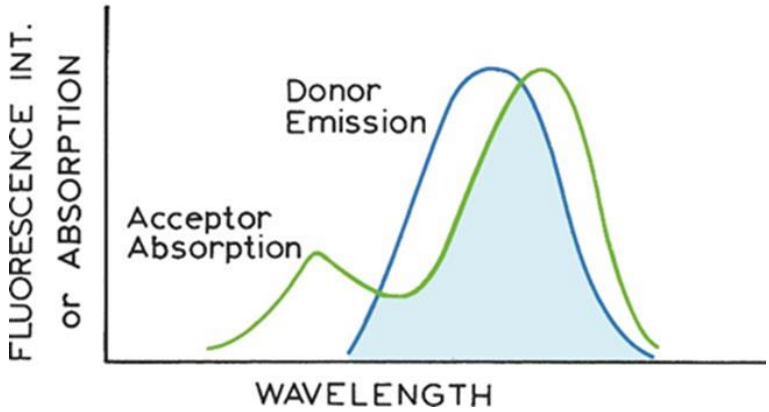

Figure 1.4 Spectral overlap for fluorescence resonance energy transfer (FRET) [2].

b. PET

A Photoinduced electron transfer (PET) process occurs when receptor or analyte has either highest occupied molecular orbital (HOMO) or the lowest unoccupied molecular orbital (LUMO) between HOMO and LUMO energy gap of the

fluorophore which acts as either a photoexcited electron acceptor or donor, respectively. As an acceptor, the excited fluorophore will have its half-filled HOMO accepting an electron transferred from the HOMO level of the other unit (Figure 1.5 left). As a donor, the excited electron in the LUMO of the fluorophore will transfer to the LUMO level of the other unit (Figure 1.5 right). The electron transfer process is a non-radiative process which results in quenching of the fluorescence. A "turn off" and "turn on" fluorescent sensor can thus be designed based on promoting or inhibiting the PET process.

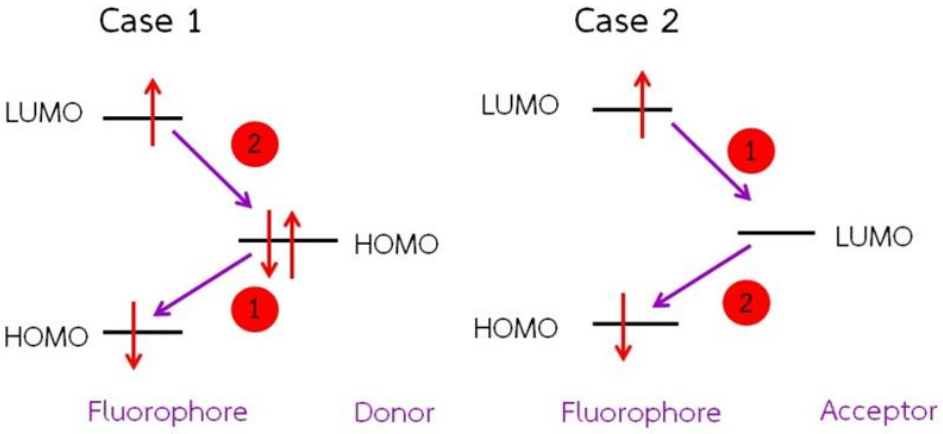

Figure 1.5 Principal photophysics of PET.

c. ICT

The initial most stable excited state of S_1 is sometime called locally excited (LE) state. In certain cases, a molecule in LE state may undergoes another geometrical relaxation along with redistribution of electron density, especially when the molecule contains both electron donating and withdrawing groups connected via π-conjugated system. The relaxation process generates a new lower energy excited state called internal charge transfer (ICT) state having very different geometry and dipole moment from the LE state (Figure 1.6). The ICT state can then relax to the ground state either by radiative or non-radiative decay. Depending on the energy band gap, this relaxation may give light within or outside the visible light spectrum. [4-6] If detectable, this emission from the ICT state is at a longer wavelength and enhanced by polar solvent as the ICT excited state more populated by the solvent stabilization. Due to multistep

process, ICT emission usually has lower fluorescence quantum yield compared with LE state. A “turn off” or “turn on” or “wavelength shift” fluorescent sensor can be designed based on the degree of the ICT process.

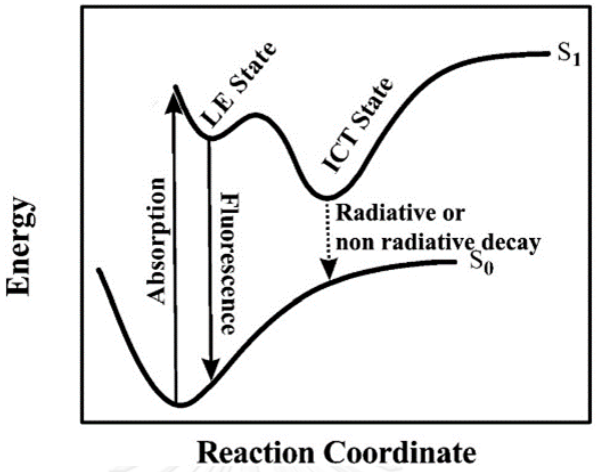

Figure 1.6 Potential energy surfaces of the ground state (S_0) is excited to S_1 then relaxed to LE, and ICT state.

d. ESIPT

The excited state intramolecular proton transfer (ESIPT) process generally associates with the transfer of a proton from a hydroxyl (or amino) group to a carbonyl oxygen (or imine nitrogen) through a six- or five-membered ring hydrogen bonding configuration intermediate. [7] The classic example of the ESIPT photophysical process was observed for 2-(20-hydroxyphenyl)-benzoxazole (**HBO**) as in Figure 1.7. After irradiation, the excited **HBO** in enol form (E*) is converted to the excited keto form (K*) in the sub picosecond time scale resulting in significantly red shift emission compared with the absorption and unusually large Stoke shift. A large Stoke shift is beneficial in fluorescence sensing to avoid the self-absorption or the inner filter effect. This ESIPT process is thus a useful in designing a fluorescent sensor with a large wavelength shift.

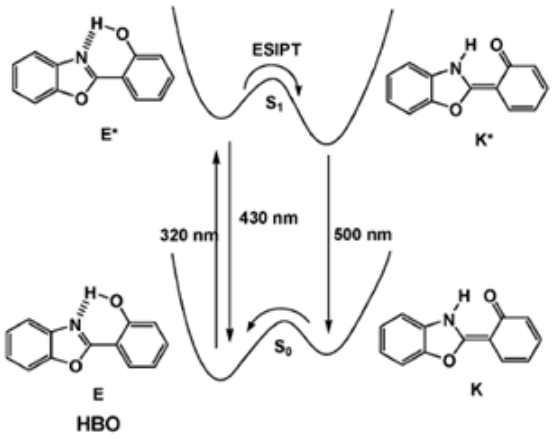

Figure 1.7 Principal photophysics of ESIPT illustrated by 2-(20-hydroxyphenyl)-benzoxazole (**HBO**) [7].

1.4 Literature reviews

Fluorescent sensors for anions have recently been extensively studied with main objectives for high selectivity and sensitivity that allows detection a designated anion at sufficiently low concentration. The aim of this section is to briefly overview progress in developments of fluorescent sensors for nucleophilic or basic anions, i.e. fluoride (F^-), sulfite (SO_3^{2-}), phosphate (PO_4^{3-}) and cyanide (CN^-), reported during the past few decades. More focus will be paid to the development of fluorescent sensors for the highly toxic cyanide ion based on indolium salts which are closely related to this thesis work.

1.4.1 Fluorescent sensors for anions

a. Fluoride anion (F^-)

The advantages of fluoride in dental health is already known, but high concentration of fluoride displayed the toxicity such as kidney failure and debilitating skeletal defects. In 2010, Gunnlaugsson [8] used thiourea receptor which connecting with 4-amino-1,8-naphthalimide, a highly colored fluorescent dye, for fluoride detection. This probe showed color change from light yellow to deep purple upon fluoride addition (≥2 equiv). The proposed mechanism is the deprotonation of the amino NH. The rising of the charge density on the amino nitrogen exhibited the push–

pull character of the ICT and confirmed with addition of tetrabutylammonium (TBA) hydroxide to give the same color change.

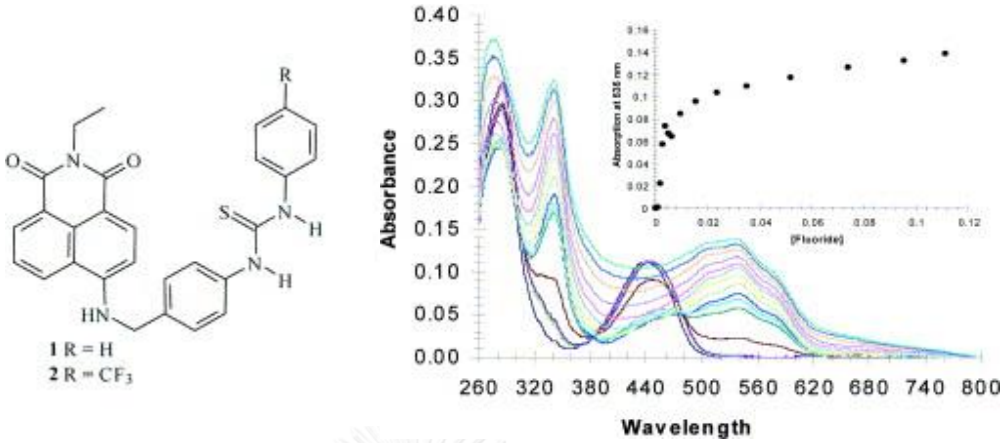

Figure 1.8 Structures of fluoride probes and changes in the absorption spectra upon addition of fluoride; inset: the absorbance change at 525 nm as a function of [F^-] [8].

In 2010, HU and coworker [9] reported fluoride probe based on the fluoride cleavage of siloxane bond (S-O). The probe which has poor solubility in water but can be solubilized by a micellar CTAB solution shows only blue-violet fluorescence, which was almost identical to the emission of the enol form of the probe. Upon addition of fluoride ions, the Si-O bond of the probe is immediately cleaved, to give an excited-state intramolecular proton transfer (ESIPT) compound, which exhibits a bright yellow emission in water (Figure 1.9).

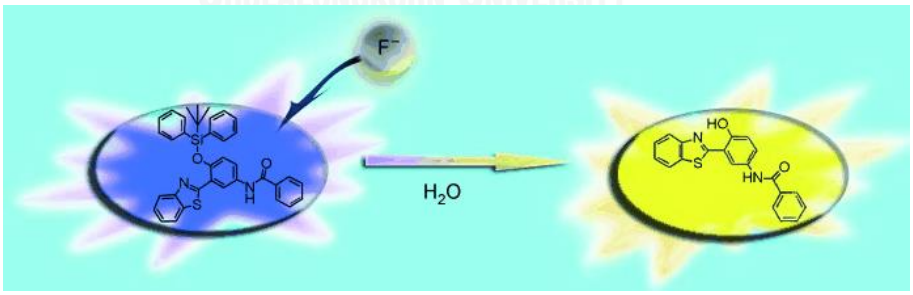

Figure 1.9 Proposed siloxane cleavage mechanism used in fluoride sensor [9].

b. Sulfites (SO_3^{2-} and HSO_3^{2-})

Sulfite is used as an additive for food and beverages industrials for antioxidant and antimicrobial but it can be toxic at even at low concentration to sensitive people. In 2012, Guo et al. reported a fluorescence probe for bisulfite anion by using the

addition reaction of bisulfite on aldehyde to generate hydrogen bonded inhibition of C=N isomerization (Figure 1.10). In DMSO–acetate buffer (0.1 M, pH 5.0, 1:1, v/v), the probe possessed very weak fluorescence at 535 nm due to the C=N isomerization. The fluorescence intensity increased upon bisulfite addition generating the product prompting hydrogen bond to inhibit the C=N isomerization.

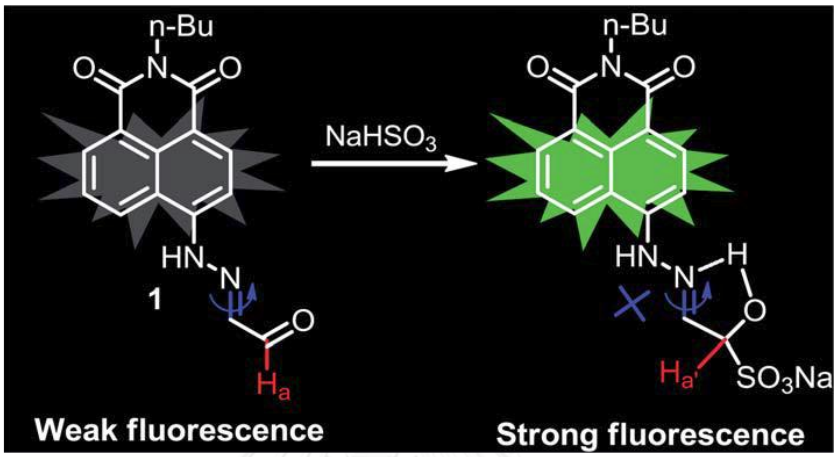

Figure 1.10 Proposed sensing mechanism of sensing probe for HSO_3^- [10].

In 2013, Du et al. [11] reported the fluorescein which containing bislevulinyl groups (**FL**) as the sulfite receptor. The proposed mechanism of this probe started with the attack of sulfite ion on the terminal carbonyl group leading to the cleavage of the ester bond to release the highly fluorescent fluorescein giving a turn on fluorescence response (Figure 1.11). This probe was applied to quantitative detection of sulfite in white wine, which gave agreeable results to the standard method.

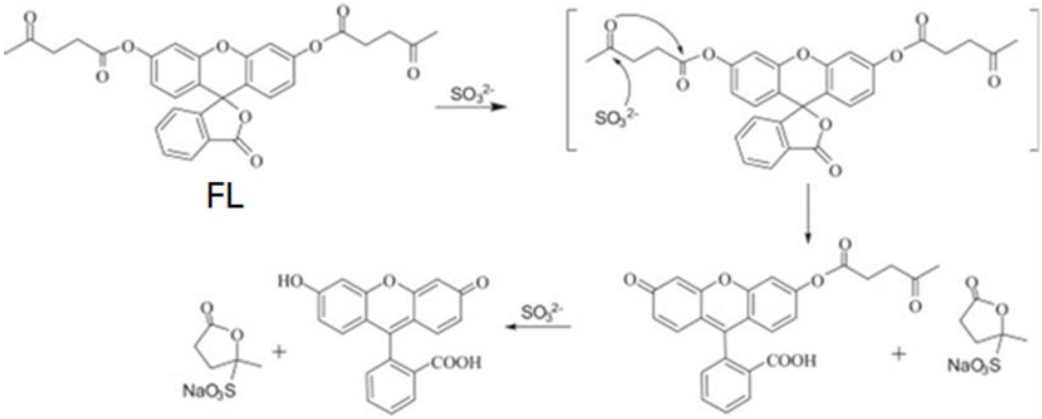

Figure 1.11 Reaction mechanism between **FL** and SO_3^{2-}[11].

c. Phosphates (PO_4^{3-}, $ROPO_3^{2-}$ and $(RO)_2PO_2^-$)

Phosphates are essential part organic molecule that play an important role in many biological processes and used in medicines [12, 13]. In 2003, Bencini et al. [14] reported a new polyammonium receptor (**$[H_6L]^{6+}$**) for adenosine triphosphate (ATP) detection. The addition ATP to a solution of the probe at pH 6.0 leads to a linear decrease of the fluorescence emission attributed to multiple hydrogen bondings between **$[H_6L]^{6+}$** and ATP ($P\text{-}O^{-}\cdots H_2N^{+}$). Its highly pH sensitive property is the major disadvantage of this probe.

In 2003, Bencini et al. [14] reported a new polyammonium receptor (**$[H_6L]^{6+}$**) (Figure 1.12) for adenosine triphosphate (ATP) detection. The addition ATP to a solution of probe at pH 6.0 leads to a linear decrease of the fluorescence emission. The hydrogen bonding interactions was used to explain the binding reaction beteen **$[H_6L]^{6+}$** and ATP ($P\text{-}O^{-}\cdots H_2N^{+}$). The disadvantage of this probe is the deprotonation of the **$[H_6L]^{6+}$** cation from the basic condition leads to the observed interfered fluorescence quenching.

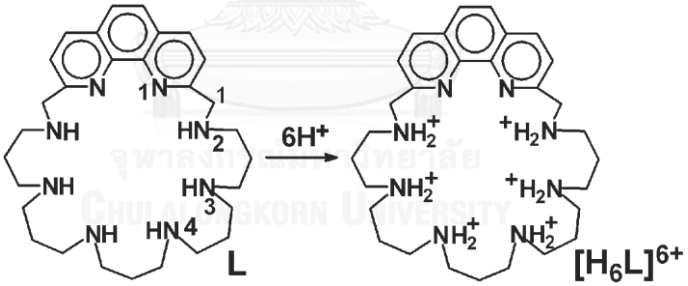

Figure 1.12 Structure of phosphate sensing probe $[H_6L]^{6+}$ [14].

In 2010, Hamachi et al. [15] reported a new ratiometric chemosensors for zinc cation form the complexes of coumarin-xanthene (**CX1** and **CX2**). This work used coumarin fluorophores as the FRET donors and binuclear zinc complex as the FRET acceptor to give the ratiometric chemosensors. When nucleoside polyphosphates ATP bound with zinc, the probes gave strong FRET signal. These chemosensors were used in a fluorescence-imaging study of the stimulus-responsive concentration change of ATP inside living cells, as an indicator of the cellular energy level (Figure 1.13).

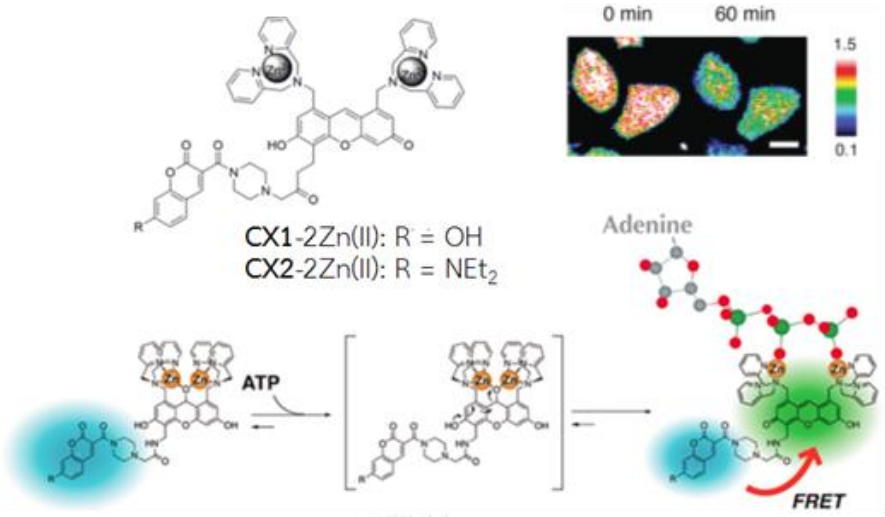

Figure 1.13 Structures of **CX1**, **CX2** and their proposed complexes with Zn^{2+} [15].

d. Cyanide (CN^-)

Cyanide is extremely toxic to human even at very low concentration, that leads to a state of histotoxic anoxia and death [16]. However, it is still widely used in several industries such as metal mining, metal extraction, electroplating, jewellery manufacturing, and X-ray film recovery [17]. Water-soluble cyanide salts are ones of the most lethal contamination and poisoning [18, 19]. WHO limits the maximum contamination of cyanide in drinking water no greater than 1.9 μM [20].

In 2005, García et al. [21] reported a polymer for sensing cyanide anion in water based on pyrylium cation. Due to the addition of NaCN, the yellow films containing pyrylium cation was changed to red films and the absorption band at 537 nm band increased with the cyanide concentration. This film was easily recovered by washing the film with aqueous acidic solutions to give original yellow color. The combination of suitable chromogenic systems and polymeric materials could lead to new sensory systems for the development of reusable colorimetric easy-to-use in situ naked-eye chemosensors for target species of interest in water. This probe showed poor sensitivity with limit of detection at 4 mM. However, this probe was highly selective with cyanide over the Cl^-, Br^-, I^-, NO_3^-, $H_2PO_4^-$, SO_4^{2-} and SCN^- anions (Figure 1.14).

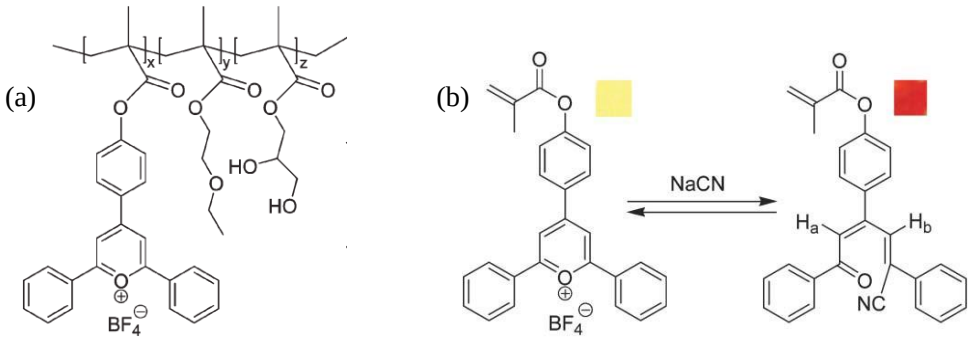

Figure 1.14 (a) Structure of cyanide sensing polymer and (b) cyanide sensing mechanism of this monomer [21].

In 2013, Zade et al. [22] used 3′-dicyanovinyl terthiophene (**DT**) as a cyanide fluorescent sensor. In THF aqueous solution, **DT** showed selectivity toward cyanide ion over other anions such as AcO^-, F^-, Cl^-, Br^-, NO_2^-, N_3^-, HS^- and ClO_4^-. The nucleophilic addition of a cyanide anion to the dicyanovinyl group inhibited an intramolecular charge transfer (ICT) and gave the colorimetric and fluorimetric responses (Figure 1.15).

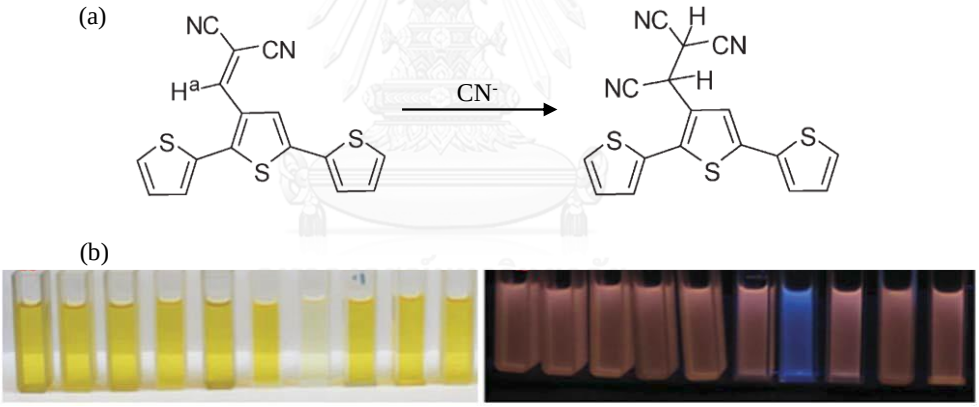

Figure 1.15 (a) **P**roposed mechanism of cyanide sensing of DT (b) colorimetric and (c) fluorimetric responses of DT (30 μM) in the presence of 20 equiv. of different anions (from left: blank, AcO^-, F^-, Cl^-, Br^-, NO_2^-, N_3^-, HS^- and ClO_4^-) [22].

In 2014, Niamnont et al. [23] reported cyanide turn-on fluorescent sensors for anion containing phenylene-ethynylene conjugated system and salicylaldehyde receptor (**S1**-**S3**) (Figure 1.16). All compounds exhibited selective turn-on fluorescence signal upon the addition of cyanide anion in aqueous media. **S3** displayed the highest sensitivity due to its low initial fluorescence quantum yield. The detection limit of 10 was 1.6 μM (42 ppb). Paper-based solid state sensor for cyanide ion was also fabricated

from **S3** (Figure 1.17). The naked eye detection of cyanide anion down to 5 nmol was achieved on filter paper using elution technique.

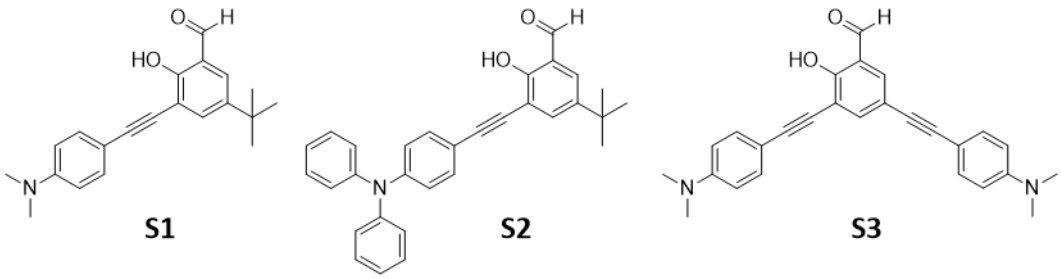

Figure 1.16 Molecular structures of **S1**-**S3** [23].

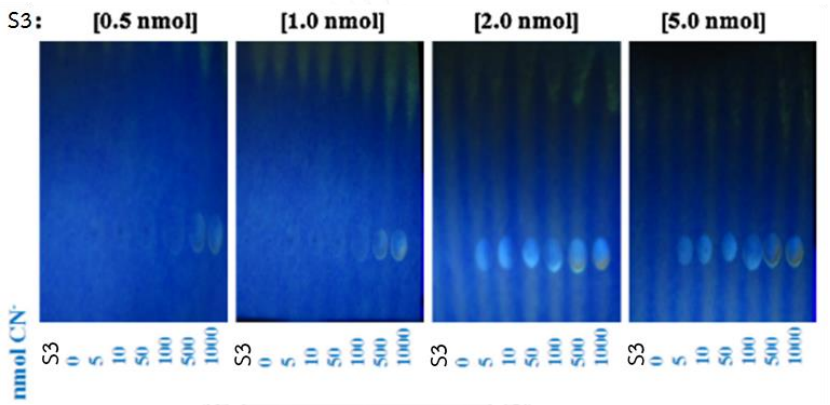

Figure 1.17 Photographic images for paper-based detection of cyanide [23].

1.4.2 Fluorescent sensors from indolium salts

The indolium group has recently emerged as one of the most sensitive probes for metal [24-28] and anion [29] especially cyanide ion with detection capability in both fluorometric and colorimetric modes [30, 31]. The strong electron withdrawing indolium conjugated with an electron donating unit can install an ICT quenching process in the fluorophore. The conversion of indolium to a group having less electron withdrawing ability has been implemented in turn on fluorescence mechanism for several analytes. In 2010, Yan et al. [32] reported a novel boronate-functioned styryl dye, **BSD**, as a colorimetric sensor for hydrogen peroxide. The transformation of arylboronate to phenolate by $H_2O_2^-$ in basic range, resulting in the release of the cyanine dye which has strong intramolecular charge transfer (ICT) absorption band. There is almost no interference due to the specific deprotection of arylboronate group

by H_2O_2. This sensor was applied to the detection of hydrogen peroxide in rain water. (Figure 1.18)

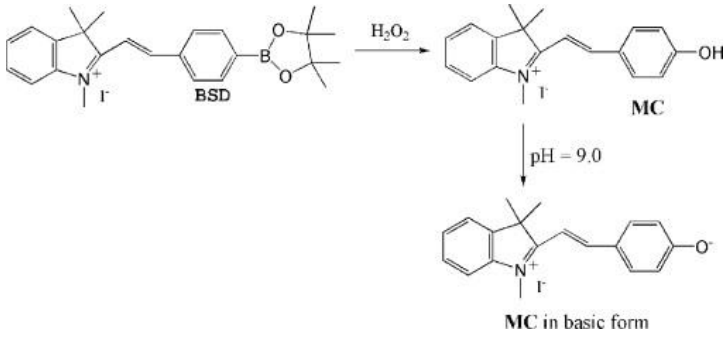

Figure 1.18 Reaction mechanism of the detection of H_2O_2 with **BSD** [32].

In 2015, Yang et al. [33] reported the rhodamine-spiropyran probe, termed **Rhod-SP**, for monitoring Cu^{2+} in lysosomes. **Rhod-SP** contains spiropyran as a proton recognition unit for switching capability and rhodamine fluorophore for signal transduction. After the spiropyran unit was activated by protonation, the Cu^{2+} collaborative coordination with C=O and C=N promotes rhodamine ring-opening and shows a turn on fluorescence response (Figure 1.19).

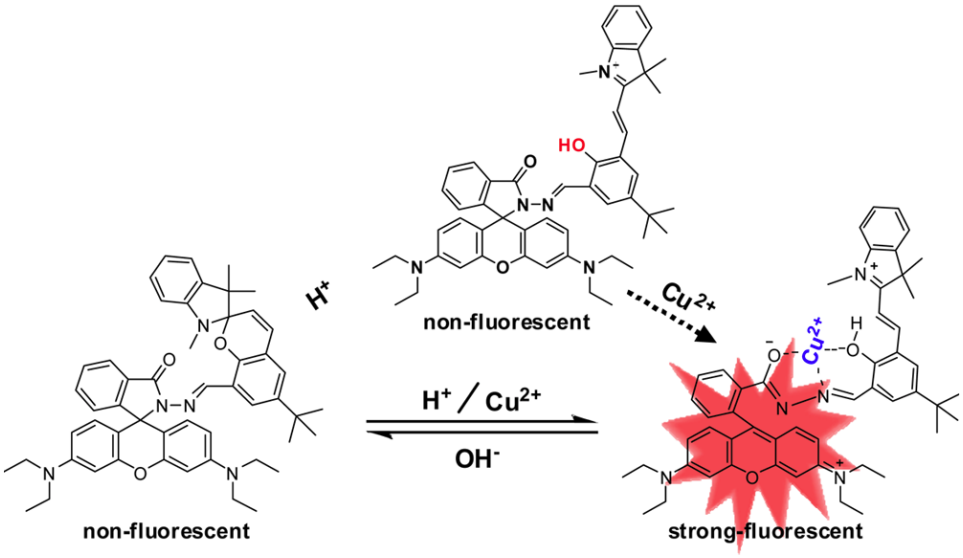

Figure 1.19 Proposed mechanism of fluorescence response of **Rhod-SP** by binding of H^+ and Cu^{2+} [33].

In 2016, Wu et al. [34] repoted a novel cyanine dye containing pyrene (**Py-Cy)**, for hypochlorite (ClO^-) detection. ClO^- cleaved the double bond between pyrene and idolium in the molecular structure of pyrene-indolium which resulting in a strong turn-on fluorescence signal (**Figure 1.20**). This probe was successfully applied in the detection of hypochlorite in real samples and cell imaging.

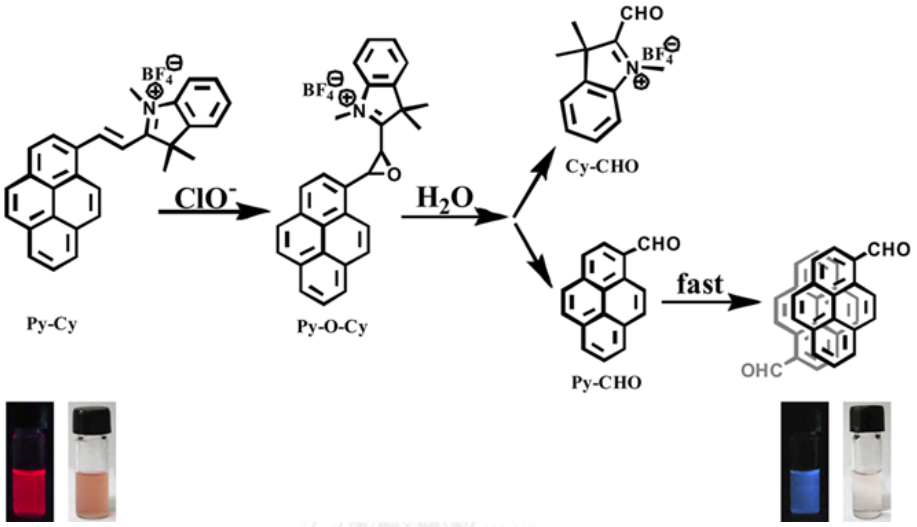

Figure 1.20 Ratiometric fluorescent response of **Py-Cy** to hypochlorite and its response mechanism [34].

1.4.3 Fluorescent sensor for cyanide detection from indolium salt

In 2011, Shiraishi et al. [35] developed a cyanide fluorescent sensor based on coumarin–spiropyran probe (**CS**). **CS** was non-fluorescent that became highly fluorescent with a blue emission under UV light, upon the addition of cyanide anion to its cyanine form (Figure 1.21). The detection limit reported was 0.5 μM in a pH 9.3 (cyclohexylamino)ethanesulfonic acid (CHES) buffered water/acetonitrile mixtures (8:2 v/v).

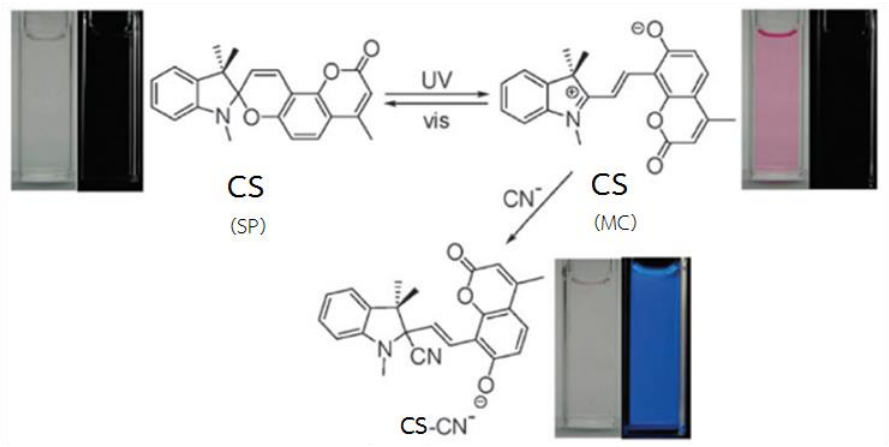

Figure 1.21 Cyanide sensing mechanism of **CS** [35].

In 2011, Guo et al. [36] reported a ratiometric fluorescent sensor for cyanide based on hybrid coumarin–indolium dye containing indolium group (**CIN**). The addition of cyanide anion to the indolium group changed the fluorescence emission of the dye from dim red to strong blue (Figure 1.22). The intensity ratio of two well-separated emission peaks at 514 nm and 630 nm was well correlated with the cyanide concentration. The detection limit for cyanide was determined as 0.6 μM in methanol /Tris-HCl buffer (10 mM, pH = 9.3, 1:1, v/v).

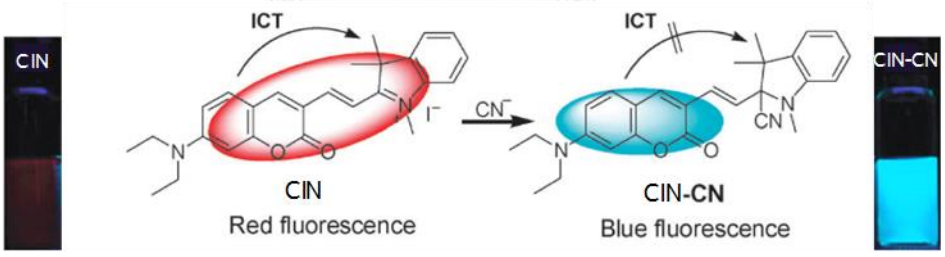

Figure 1.22 Cyanide sensing mechanism of coumarin–indolium conjugate [36].

In 2014, Shiraishi et al. [37] reported a comparative sensing study between the compound **CIN,** previously reported by Guo et al. [36], and its chloro derivative (**CINCl**) (Figure 1.23). These dyes exhibited selective emission enhancement by cyanide anion with a similar detection limits of 0.4 μM measured in a buffered water/acetonitrile mixture (7/3 v/v; CHES 100 mM, pH 9.0). The report also claimed that electron withdrawing chloride group increased the electrophilicity of the indolium carbon that accelerates the reaction with cyanide, allowing a faster detection of cyanide (< 1 minute).

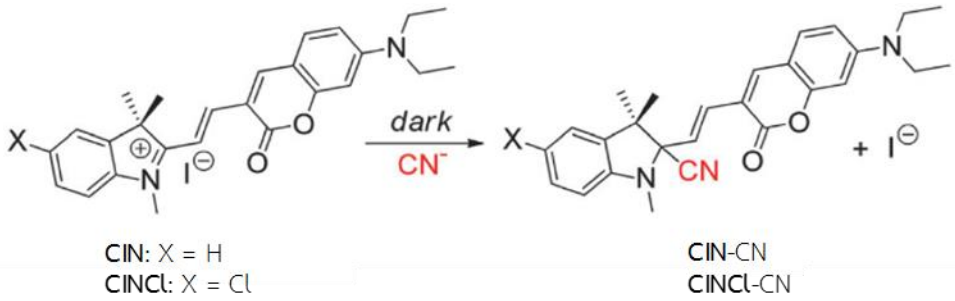

Figure 1.23 Cyanide sensing mechanism of indolium-coumarin conjugates [37].

In 2014, Peng et al. [38] developed three cyanide fluorescent sensors **CH1-CH3** based on cyanine dye containing coumarin unit (Figure 1.24). All compounds gave good sensitivity and high selectivity toward cyanide, with the detection limits of 9-33 μM. **CH3** was found to be more reactive than the other two compounds that allowed the naked eye detection of cyanide in 3 minutes.

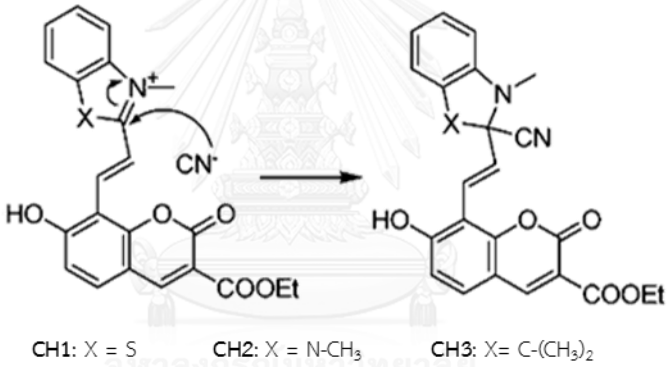

Figure 1.24 Cyanide sensing mechanism of **CH1**-**CH3** [38].

In 2014, Zhou et al. [39] reported a colorimetric and fluorescent sensor for cyanide based on the cyanine dye containing anthracene moiety (**AH**). The reaction between **AH** and cyanide is extremely fast completed within 1 second. The addition of cyanide anion to the indolium group showed blue fluorescent emission and the solution color changed from red to colorless clearly observable by naked eye (Figure 1.25). The detection limit was also very low, 59 nM, measured in ethanol/Tris-HCl buffer (10 mM, pH = 7.4, 2:8, v/v). Interestingly, the probe can track the intracellular cyanide in living human breast cancer GES cells (Figure 1.26)

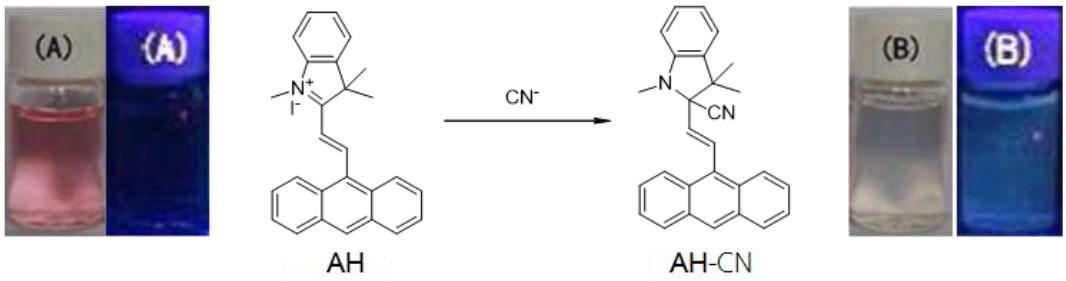

Figure 1.25 Cyanide sensing mechanism of conjugated anthracene-hemicyanine probe [39].

Figure 1.26 (A) Bright-field transmission imaging of GES cells and fluorescence imaging of live GES cells with probe **AH** (30 μM) (B) before and (C) after treated with CN^- (45 μM) for 30 min [39].

In 2015, Song et al. [40] reported a colorimetric and "turn-on" fluorescent probe **TI** for the detection of cyanide anions. Cyanide was detected via the nucleophilic addition to the indolium group which acted as the receptor for cyanide, resulted in a change from a purple color to colorless and an enhancement in fluorescence. The probe showed a high sensitivity and selectivity for cyanide anion over other common anionic species in aqueous ethanol solution. The limit of detection in EtOH/Tris-HCl buffer pH 7.4 (10.0 mM, 4:6, v/v) was as low as 21 nM. A live cell imaging experiment from this probe for tracing cyanide anions in biological systems is developed. (Figure 1.27)

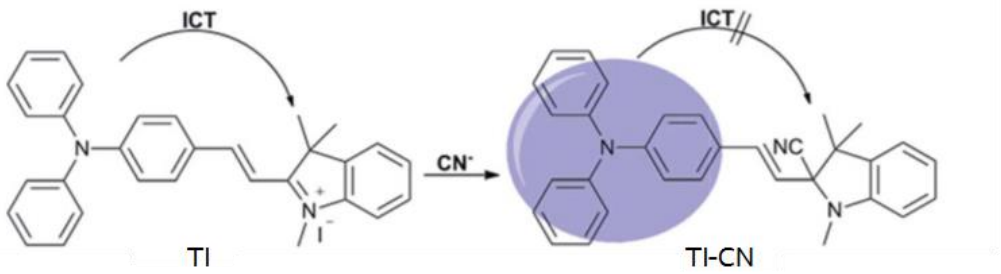

Figure 1.27 Structure of **TI** and graphic of cyanide sensing mechanism [40].

In 2016, Yang et al. [41] reported a cyanine dye (**Cac**) containing electron donor carbazole group for colorimetric and ratiometric fluorescent sensor for cyanide detection. Upon treatment with cyanide, **Cac** displayed the fluorescence ratiometric response, with the emission wavelength displaying a very large emission shift (214 nm). The detection of cyanide was performed via the nucleophilic addition of cyanide anion to the indolium receptor of the probe which resulted in stalling of the ICT process, inducing the ratiometric fluorescence and color change. (Figure 1.28) Furthermore, competitive anions did not cause any significant changes both in color and emission intensity, indicating the high selectivity of the sensor to CN^-. The detection limit of this probe is 0.4 μM, measured in DMSO-buffer pH 7.4 (Tris-HCl, 10.0 mM, 6:4, v/v).

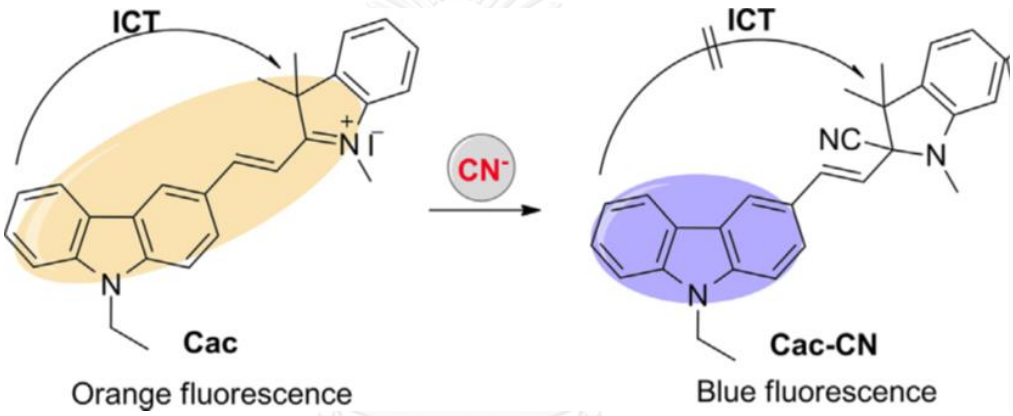

Figure 1.28 Proposed cyanide sensing mechanism of **Cac** [41].

In 2016, Chao et al. [42] reported 1,1-dimethyl-3-ethyl-2-(2-(N-ethyl-carbazol-3-yl)-vinyl)-1H-benzo[e]indolium iodide as a ratiometric emission fluorescent probe for monitoring cyanide ion (Figure 1.29). The detection of cyanide is performed via the nucleophilic attack of cyanide to the benzo[e]indolium which is the cyanide receptor of the probe, resulting in the fluorescence ratiometric and the color change. The titration experiments for CN^- showed high selectivity, sensitivity and good stability in DMSO solvent system. The CN^- detection limit of the probe was 0.23 μM. Furthermore, the probe has cell membrane permeability and was applied successfully to rapidly detect CN^- in living cells.

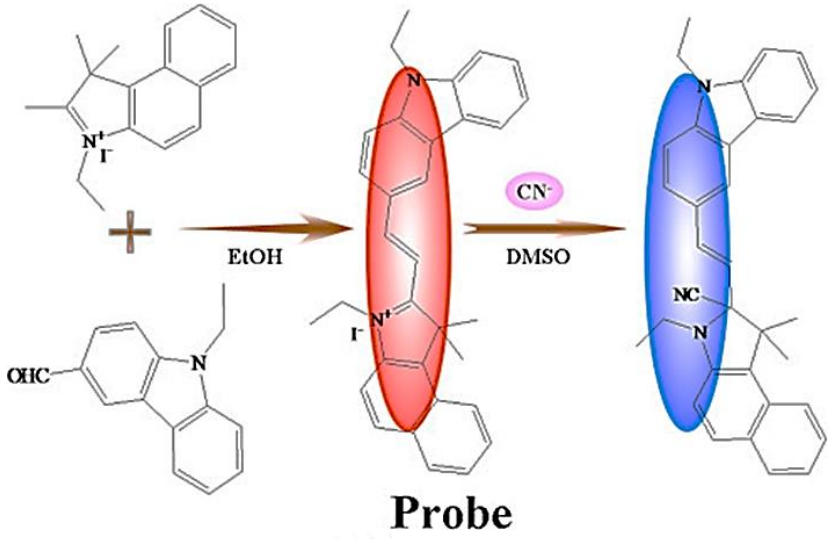

Figure 1.29 Synthesis of cyanide probe and proposed sensing mechanism [42].

1.5 Hypotheses and objectives

A new series of cyanine dyes (Figure 1.30) containing phenolate electron donors conjugated with indolium electron acceptor are designed and studied for a cyanide turn-on fluorescent sensors. The indolium group is used as the cyanide receptor with fluorescent quenching capability via intramolecular charge transfer (ICT) process between. The synthesized compounds will be evaluated and optimized to obtain high sensitivity and selectivity for cyanide sensing in aqueous media. Development of the most sensitive compound for naked eye detection of cyanide for convenient use in the on-site analysis is also another key objective of this work.

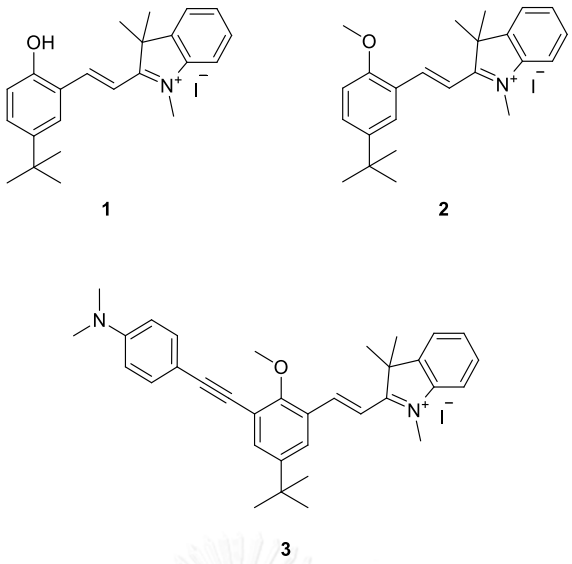

Figure 1.30 Target molecules.

CHAPTER II

EXPERIMENT

2.1 Apparatus, reagents and chemicals

Iodomethane, copper (I) iodide, triphenylphosphine, quinine sulfate, bis(triphenylphosphine) palladium(II) dichloride ($PdCl_2(PPh_3)_2$), were purchased from Aldrich. Triethylamine and solvents were purchased from Lab-scan, Thailand. The solvents used for running the reactions such as dimethylformamide and tetrahydrofuran were reagent grade stored over 4A molecular sieves. In anhydrous reactions, ethanol was dried by distillation over sodium before use according to the standard procedures. All reactions were conducted under positive pressure of N_2 filled in rubber balloons. Solvents used for extraction and chromatography such as dichloromethane, hexane, ethyl acetate and methanol were commercial grade and distilled before use. All column chromatography was carried out using Merck silica gel 60 (70-230 mesh). Thin layer chromatography (TLC) was performed on silica gel plates (Merck F245). Milli-Q water was used in all aqueous analytical experiments unless specified otherwise.

2.2 Analytical instruments

^{1}H NMR spectra were acquired on a Varian Mercury NMR spectrometer at 400 MHz and ^{13}C NMR spectra were obtained from a Bruker NMR spectrometer at 100 MHz. The HRMS spectra were measured on an electrospray ionization mass spectrometer (microTOF, Bruker Daltonics). Absorption spectra were measured by using Varian Cary 50 UV-vis spectrophotometer. Fluorescence spectra were recorded on a Varian Cary Eclipse spectrofluorometer. The absorption and emission spectra were acquired from methanol and aqueous solution in a quart cuvette with 1 cm path length.

2.3 Synthesis

2.3.1 Synthesis of 6)-tert-butyl-(1',3',3'-trimethylspiro]chromene-2,2'-indoline[

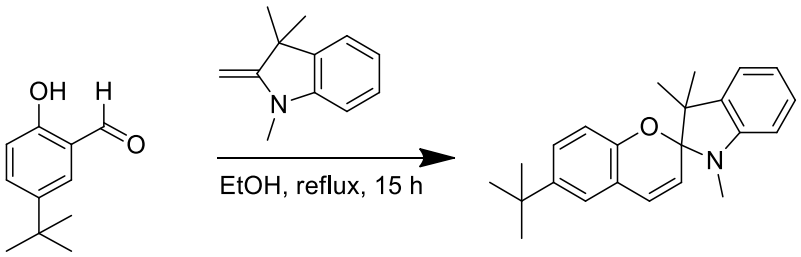

A solution of 2,3,3-trimethylindolenine (**1b**) (2.60 g, 16.12 mmol) and iodomethane (4.59 g, 32.24 mmol) in acetonitrile (30 mL) was refluxed for 18 h. The solvent was evaporated under vacuum and the residue was extracted with diethyl ether (100 mL), yielding a powder. The solid was filtered off, washed with diethyl ether (2 × 100 mL), and then dried under high vacuum. The resulting solid was then added to 3M KOH (100 mL), stirred for 30 min and extracted with diethyl ether to afford 1,3,3-trimethyl-2-methyleneindoline (2.30 g, 82%). Next, 1,3,3-trimethyl-2-methyleneindoline (1.00 g, 5.77 mmol) was dissolved in dry ethanol (80 mL) and refluxed with 5-tert-butyl-2-hydroxybenzaldehyde (1.03 g, 5.77 mmol) under nitrogen atmosphere for 15 h. The reaction mixture was cooled to room temperature and evaporated under reduced pressure. The remaining solid was dissolved in CH_2Cl_2 (30 mL), washed with 3 M NaOH (50 mL) and extracted with CH_2Cl_2 (3 × 50 mL). The combined organic was evaporated under reduced pressure then purified by silica gel column chromatography using ethyl acetate-hexane (2:97) as the eluent to afford **1b** as a colorless viscous oil (1.2 g, 60% yield).; ^{1}H NMR (CD_3OD, 400 MHz): δ (ppm) 7.19 - 7.09 (m, 1H), 7.05 (d, *J* = 7.2 Hz, 1H), 6.94 (d, *J* = 10.2 Hz, 1H), 6.79 (t, *J* = 7.4 Hz, 1H), 6.55 (dd, *J* = 20.6, 8.0 Hz, 2H), 5.73 (d, *J* = 10.2 Hz, 1H), 3.33 (s, 3H), 2.71 (s, 3H), 1.29 (s, 9H), 1.16 (s, 3H).^{13}C NMR (CD_3OD, 100 MHz) δ 153.6, 149.7, 144.1, 138.1, 131.1, 128.5, 127.7, 124.7, 122.4, 120.1, 120.1, 119.6, 115.0, 107.8, 105.6, 52.6, 34.8, 31.9, 29.2, 26.3, 20.5. HRMS calcd. for [**1b**+H]$^+$: $C_{23}H_{28}NO^+$ = 334.2165; found 334.2168).

2.3.2 Synthesis of 5)-tert-butyl-(2-methoxybenzaldehyde

5-tert-butyl-2-hydroxybenzaldehyde (**4**) (1.78 g, 10 mmol) was dissolved in dimethylformamide (25 mL) by stirring with a magnetic bar in a sealed tube at room temperature. The solution was added with potassium carbonate (1.35 g, 10 mmol) and the mixture was stirred for 30 minutes, before adding with iodomethane (2.84 g, 20 mmol). The stirring was continued for 20 hours and then extracted with water (100 mL). The aqueous phase was washed with diethyl ether (2×100 mL). The combined organic phase was dried over $MgSO_4$ and evaporated by rotary evaporator to afford **4** as a brown viscous liquid (1.75 g, 91% yield).; ^{1}H NMR ($CDCl_3$, 400 MHz): δ (ppm) 10.31 (s, 1H), 7.71 (s, 1H), 7.42 (d, J = 8.6 Hz, 1H), 6.78 (d, J =8.74 Hz, 1H), 3.72 (s, 3H), 1.15 (s, 9H).; ^{13}C NMR ($CDCl_3$, 100 MHz): δ (ppm) 189.2, 159.6, 143.0, 132.8, 124.3, 123.9, 111.2, 55.2, 33.8, 30.9.

2.3.3 Synthesis of (*E*)-2-(5-(tert-butyl)-2-methoxystyryl)-1,3,3-trimethyl-3H-indol-1-ium iodide

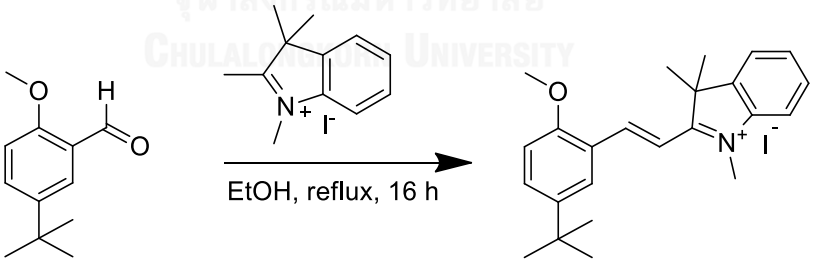

5-*tert*-butyl-2-methoxybenzaldehyde (**2**) (1.92 mg, 10 mmol) was mixed with 1-methyl-2,3,3-trimethyl-3H-indolium iodide (1.74 mg, 10 mmol) in anhydrous ethanol (20 mL). After refluxing for 20 h, the reaction produced orange crystals, which were then filtered and washed with ice-cold ethanol. The crude crystals were recrystallized in dichloromethane/hexane to give the desired product **2** as bright orange needle crystals (2.96 mg, 85% yield); ^{1}H NMR (CD_3OD, 400 MHz): δ (ppm) 8.68 (d, J = 16.4 Hz, 1H), 8.04 (d, J = 2.1 Hz, 1H), 7.89 – 7.63 (m, 6H), 7.19 (d, J = 8.8 Hz, 1H), 4.20 (s, 3H),

4.08 (s, 3H), 1.88 (s, 6H), 1.43 (s, 9H).; ^{13}C NMR (CD_3OD, 100 MHz): δ (ppm) 184.4, 159.8, 151.4, 145.6, 144.7, 143.2, 134.4, 130.8, 130.5, 128.6, 123.9, 123.6, 115.9, 113.5, 113.5, 56.9, 53.7, 35.2, 35.1, 31.7, 26.9. HRMS m/z calculated for **2**: $C_{24}H_{30}NO^+$ = 348.2322; found 348.2325

2.3.4 Synthesis of compound 5)-tert-butyl-(2-hydroxy-3-iodobenzaldehyde

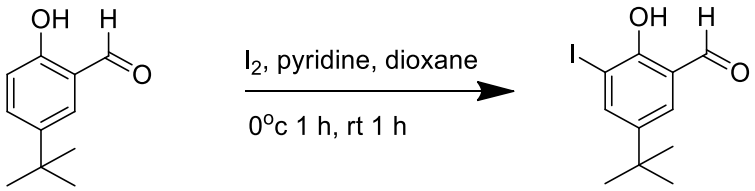

5-*tert*-butyl-2-hydroxybenzaldehyde (**5**) (2.00 g, 11.22 mmol) was dissolved in dioxane (10 mL) and pyridine (10 mL) by stirring at 0 ºC for 30 min. The solution was added with iodine (11.40 g, 44.89 mmol) and stirred for 1h in an ice bath and the stirring was continued for 1 h at room temperature. $Na_2S_2O_3$ solution (20% w/v) was added to the dark viscous residual oil until it turned light yellow. The mixture was extracted with dichloromethane (3×50 mL). The combined organic phase was washed with water (2×100 mL) and dried over anhydrous $MgSO_4$. The solution was removed under reduced pressure to afford the desired product as a brown solid (3.31 g, 97% yield). ^{1}H NMR ($CDCl_3$, 400 MHz): δ (ppm) 11.51 (s, 1H), 9.68 (s, 1H), 7.93 (s, 1H), 7.50 (s, 1H), 1.25 (s, 9H); ^{13}C NMR ($CDCl_3$, 100 MHz): δ (ppm) 196.1, 158.1, 144.8, 143.6, 130.6, 119.9, 85.5, 34.1, 31.3.

2.3.5 Synthesis of compound 5)-tert-butyl-(3-iodo-2-methoxybenzaldehyde

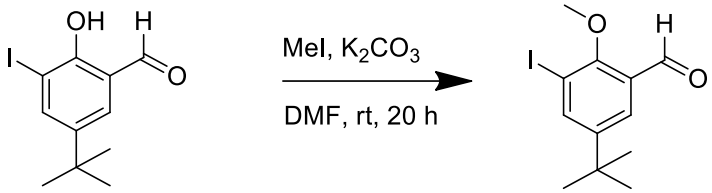

5-tert-butyl-2-hydroxy-3-iodobenzaldehyde (**6**) (2.50 g, 8 mmol) was dissolved in dimethylformamide (15 mL) by stirring with a magnetic bar in a sealed tube at room temperature. The solution was added with potassium carbonate (1.35 g, 10 mmol) and the mixture was stirred for 30 minutes, before adding with iodomethane (2.27 g, 16 mmol). The stirring was continued for 20 hours and then extracted with water (100

mL). The aqueous phase was washed with diethyl ether (2×100 mL). The combined organic phase was dried over $MgSO_4$ and evaporated by a rotary evaporator to afford **6** as a brown viscous liquid (2.55 g, 99% yield).; ^{1}H NMR ($CDCl_3$, 400 MHz): δ (ppm) 10.21 (s, 1H), 7.95 (d, *J* = 1.56 Hz, 1H), 7.75 (d, *J* = 1.64 Hz, 1H), 3.83 (s, 3H), 1.22 (s, 9H).; ^{13}C NMR ($CDCl_3$, 100 MHz): δ (ppm) 189.6, 149.8, 142.8, 141.7, 130.0, 125.9, 92.8, 63.8, 34.6, 31.1.

2.3.6 Synthesis of compound 5)-tert-butyl-(3))-4)-dimethylamino(phenyl(ethynyl-(2-methoxybenzaldehyde

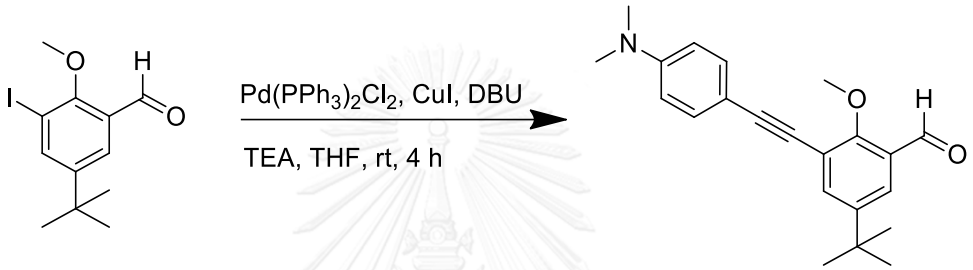

5-tert-butyl-2-methoxy-3-iodobenzaldehyde (**7**) (0.65 g, 2 mmol), $PdCl_2(PPh_3)_2$ (0.07 g, 0.1 mmol), CuI (0.008 g, 0.05 mmol), PPh_3 (0.014 g, 0.05 mmol), and 4-ethylnyl-*N*,*N*-dimethylaniline (0.44 g, 3 mmol) were dissolved in tetrahydrofuran (10 mL) and triethylamine (10 mL) by stirring with a magnetic bar in a round-bottom flask. The reaction mixture was stirred at room temperature for 4 hours. The mixture was filtered and evaporated. The residue was eluted through a silica gel column by gradient eluents starting from hexane to dichloromethane/hexane (3/1) to afford the desired product **7** as tallow solid. (0.38 g, 57% yield).; ^{1}H NMR ($CDCl_3$, 400 MHz): δ (ppm) 10.43 (*s*, 1H), 7.77 (dd, *J* = 12.8, 2.5 Hz, 2H), 7.45 (d, *J* = 8.8 Hz, 2H), 6.68 (d, *J* = 8.7 Hz, 2H), 4.16 (s, 3H), 3.00 (s, 6H), 1.32 (d, *J* = 13.0 Hz, 9H).; ^{13}C NMR ($CDCl_3$, 100 MHz): δ (ppm) 190.1, 161.7, 150.4, 146.8, 136.7, 132.6, 128.5, 124.0, 118.2, 111.9, 109.6, 96.3, 82.9, 62.5, 40.1, 34.52, 31.2.

2.3.7 Synthesis of compound)E-(2)-5)-tert-butyl-(3))-4)-dimethylamino (phenyl(ethynyl-(2-methoxystyryl-(1,3,3-trimethyl-3H-indol-1-ium iodide

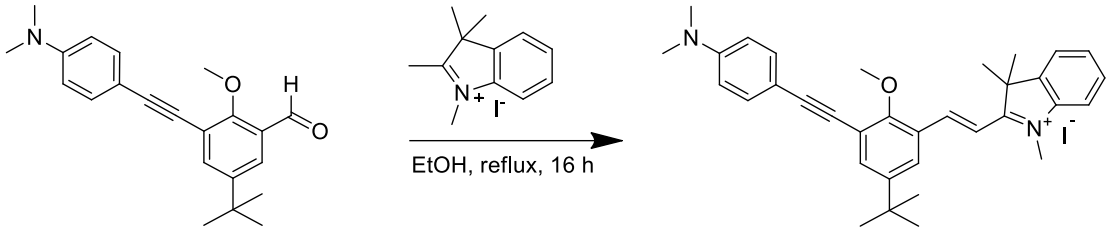

3-(4-N,N-dimethylaminophenylethynyl)-5-tert-butyl-2-methoxybenzaldehyde (**3**) (7, 100 mg, 0.30 mmol) was mixed with 1-methyl-2,3,3-trimethyl-3H-indolium (58 mg, 0.33 mmol) in anhydrous ethanol (20 mL). The reaction mixture was refluxed for 20 h, before the solvent was removed under reduced pressure. The residue was suspended in hexanes (100 mL), sonicated for 10 min then filtered off and washed with methanol (2×20 mL) to afford the desired product **3** as a brown solid (84 mg, 57% yield).; 1H NMR ($CDCl_3$, 400 MHz): δ (ppm) 8.64 (d, *J* = 16.6 Hz, 1H), 8.06 (d, *J* = 1.8 Hz, 1H), 7.88 (dd, *J* = 5.6, 3.2 Hz, 1H), 7.81 (dd, *J* = 15.1, 11.2 Hz, 3H), 7.70 (dd, *J* = 5.6, 3.1 Hz, 2H), 7.44 (d, *J* = 8.7 Hz, 2H), 6.78 (d, *J* = 8.7 Hz, 2H), 4.23 (d, *J* = 12.5 Hz, 6H), 3.03 (s, 6H), 1.90 (s, 6H), 1.45 (s, 9H).; ^{13}C NMR ($CDCl_3$, 100 MHz): δ (ppm) 184.5, 160.4, 152.2, 150.4, 149.0, 144.8, 143.3, 137.0, 133.6, 131.2, 130.6, 128.2, 126.5, 12.0, 119.6, 116.2, 114.7, 113.1, 110.7, 97.9, 83.6, 62.5, 54.0, 40.3, 35.6, 35.0, 31.6, 26.6. HRMS m/z calculated for **3**: $C_{25}H_{30}N_2O^+$ = 491.3057; found = 491.3062.

2.4 Measurement of photophysical properties

The UV-vis absorption spectra were acquired from the solutions of **1** (45 μM), **2** (45 μM) and **3** (32 μM) in methanol. The extinction coefficients (**ε**) were obtained from the solutions of **1**, **2** and **3** in the concentration range of 10-40 μM. The emission spectra were measured from the solution of **3** (10 μM) in methanol or aqueous HEPES buffer pH 6.0 (10 mM) solution containing Triton X-100 (220 μM). The excitation wavelengths used for methanol and aqueous solutions were 385 and 340 nm, respectively. The fluorescence quantum yield was determined from the solutions of **3**

in the concentration range giving the absorption < 0.1 using quinine sulfate in 0.1 M H_2SO_4 aqueous solution as a reference (Φ_F = 0.54).

2.5 Sensing study

2.5.1 In solution

The sensing studies were performed by UV-vis absorption and fluorescence spectroscopy of the solutions of probes **1**, **2** and **3** in methanol or HEPES buffer using sodium salts of various anions. Detail conditions such as concentration, solvent, mixing time and additive were specified in the corresponding results.

2.5.2 On filter paper

The solution of **3** (100 μM, 1 μL) in acetonitrile, HEPES buffer pH 6.0 (10 mM, 1 μL) and Triton X-100 (220 μM, 1 μL) were dropped successively onto the designated area of a piece of filter paper and allowed for air dry in an ambient atmosphere to generate sensing spots. The NaCN solutions (2 μL) at various concentrations were dropped on top of the sensing spots. After air-drying, the images were recorded by a digital camera under room light and black light illuminations.

2.6 Preparation of sensing alginate gel bead

2.6.1 Normal bead

Sodium alginate 1.00 g was dissolved by vigorous stirring in HEPES buffer pH 6.0 (10 mM, 40 mL) for 3 h. The stock solution of **3** (10 mM, 0.5 mL) and Triton X-100 solution (22 mM, 0.5 mL) were then added to the sodium alginate solution. The final volume of the solution was adjusted to 50 mL by the buffer solution to produce the **3**/alginate (100 μM/2% w/v) solution. The solution was degassed by sonication and left overnight at 4 ℃ to allow removal of air bubble in the solution. To form the bead, the **3**/alginate solution (10 mL) was dropped, via a syringe needle No. 26, into a low speed stirring $CaCl_2$ solution (5% w/v, 100 mL). After 3 min, scooped up the beads and rinsed with deionized water and stored for further study in milli-Q water at 4 ℃.

2.6.2 Reverse bead

Sodium alginate 1.00 g was dissolved by vigorous stirring in HEPES buffer pH 6.0 (10 mM, 80 mL) for 3 h. Triton X-100 solution (22 mM, 1.00 mL) was then added to the sodium alginate solution. The final volume of the solution was adjusted to 100 mL by the buffer solution to produce the sodium alginate (1% w/v) solution. The sodium alginate solution was degassed by sonication and left overnight at 4 °C to allow removal of air bubble. $CaCl_2$ 0.50 g was dissolved by stirring in the buffer solution (10 mM, 8 mL) for 10 minute. Triton X-100 solution (22 mM, 0.1 mL) and the stock solution of **3** (10 mM, 0.1 mL) were added to the calcium solution. The final volume of the solution was adjusted to 10 mL by the buffer solution to produce the **3**/calcium (100 μM/5% w/v) solution. The **3**/calcium solution was injected into pockets (6 mm) of bubble wrap and was then chilled at -78 °C for 10 min to give spheroid beads. The beads were unpacked into the alginate solution (100 mL) and allowed to stand for 30 second. The beads were washed with deionized water and stored in milli-Q water at 4 °C.

CHAPTER III

RESULTS AND DISSCUSSION

3.1 Synthesis and characterization

Indolium derivatives **1**, **2** and **3** (Figure 3.1) were synthesized from a Knoevenagel condensation between benzaldehyde derivatives with the methyleneindoline. Preformed methyleneindoline was required for the synthesis of compound **1**, while the preparation of **2** and **3** used the methylindolium generated in situ by heating with the aldehydes (Scheme 3.1). The coupling reactions gave **1**, **2** and **3** in 60%, 85% and 57% yields, respectively. The compounds were characterized by ^{1}H, ^{13}C NMR and ESI mass spectra (Figure A1-A17). Interestingly, ^{1}H NMR spectrum of **1** showed the signals of olefin proton with relatively smaller *J* coupling constant of 10.2 comparing with those observed for **2** and **3** (*J* = 15.1-16.6). This suggested that **1** was more likely to be in the spirocyclic form **1b** with a *cis* double bond rather than in the open chain *trans* alkene **1a**. Also, two groups of the proton signals were observed for two methyl groups on C3 of indoline ring of **1** confirming their diastereotopic nature corresponding to form **1b**, while only one proton signal was observed for those two homotopic methyl groups of **2** and **3**. With active hydroxyl group, the cyanine form **1a** was readily isomerized via cyclization to the more thermodynamically stable spiropyran form **1b** under ambient condition. This ring closure was not possible with the hydroxyl group methylated such as in **2** and **3**.

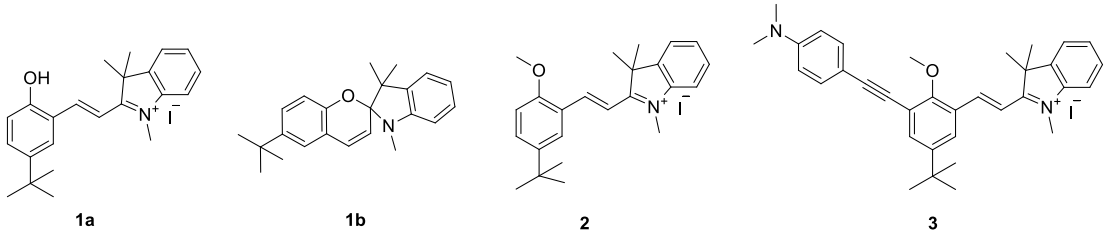

Figure 3.1 Structures of **1a**, **1b**, **2** and **3**.

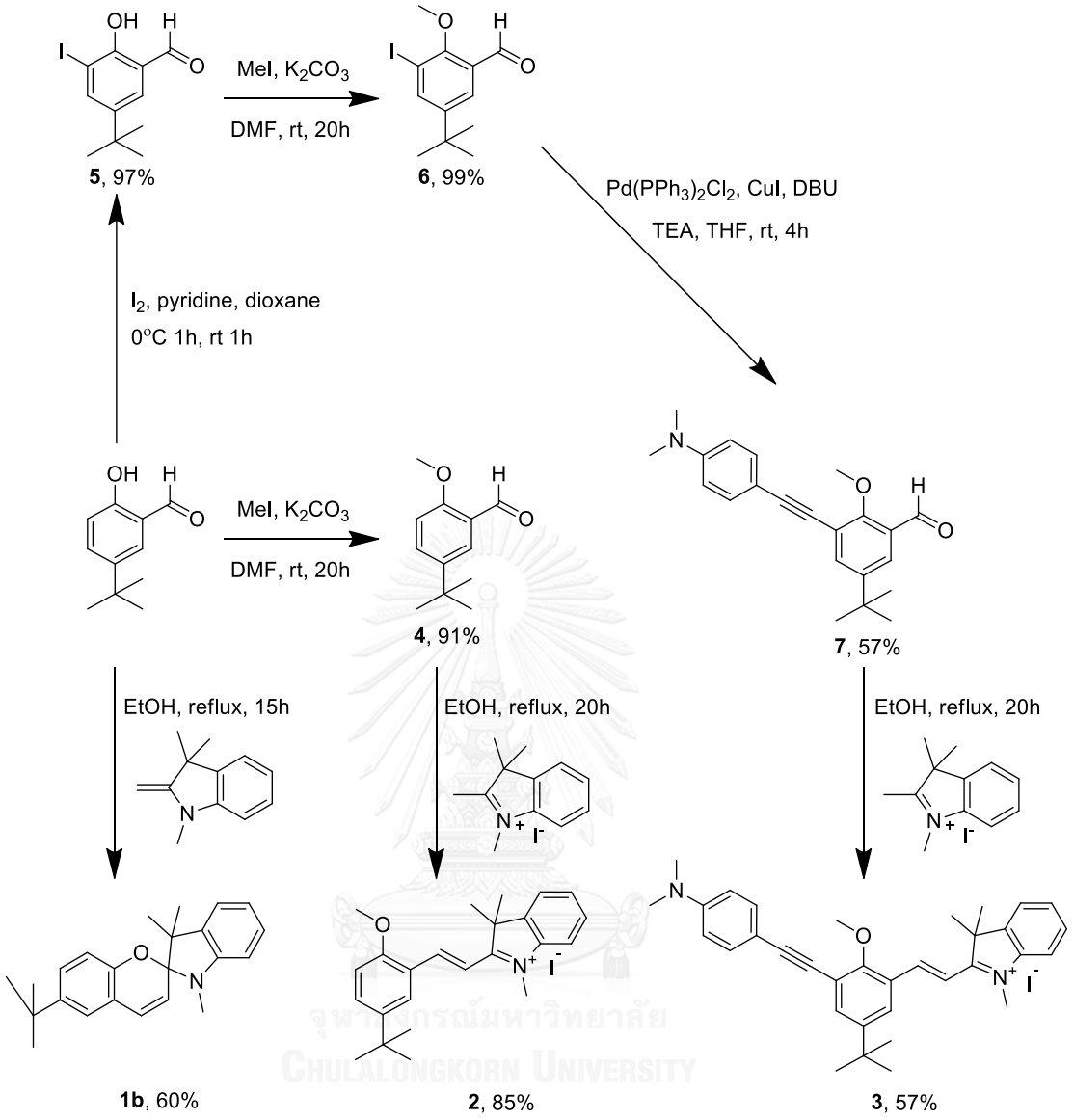

Scheme 3.1 Synthetic procedure of **1b**, **2** and **3**.

3.2 Photophysical properties

Among three compounds, only **2** was readily soluble in water while **1** and **3** soluble in polar organic solvent such as acetonitrile, ethanol and methanol. For comparison, the photophysical properties of these three compounds were studied in methanol and compiled in Table 3.1. Compounds **1** and **2** showed absorption maxima at 294 and 430 nm (λ_{max}) with the extinction coefficients (ε) of 6.81×10^3 and 1.53×10^4 $cm^{-1}M^{-1}$ respectively, but not showed fluorescent. **3** in methanol exhibited 2 absorption

bands at 341 and 397 nm (λ_{max}) with the extinction coefficients (ε) of 2.13×10^4 and 1.94×10^4 $cm^{-1}M^{-1}$, respectively. The much shorter λ_{max} of **1** confirms the shorter π-conjugated system of the spiropyran structure. While **1** and **2** did not show clear emission peaks, compound **3** gave a weak emission band with the maximum intensity at 420 nm (λ_{em}) when being excited at 340 nm (λ_{ex}). The fluorescence quantum efficiency of all compounds in methanol were very low ($\Phi_F < 0.001$) which are quite common for spiropyran and cyanine structures. [35]

Table 3.1 Photophysical properties of **1b**, **2** and **3** in methanol.

Compound	λ_{max} (nm)	log ε
1b	294	3.83
2	430	4.18
3	341, 397	4.32, 4.29

3.3 Anion sensing properties in methanol

The study of anion sensing properties of compounds **1**-**3** was started with the measurement of absorption spectra of the compounds in methanol solutions upon the addition of sodium salts of various anions) CN^-, F^-, Cl^-, Br^-, I^-, ClO_4^-, CO_3^{2-}, N_3^-, NO_2^-, NO_3^-, AcO^-, PO_4^{3-}, SCN^-, SH^-, SO_3^{2-}, and SO_4^{2-}). The original absorption peaks of **2** (Figure 3.2) and **3** (Figure 3.3) completely disappeared upon the addition of cyanide ion and noticeably decreased with some other basic anions such as acetate and carbonate.

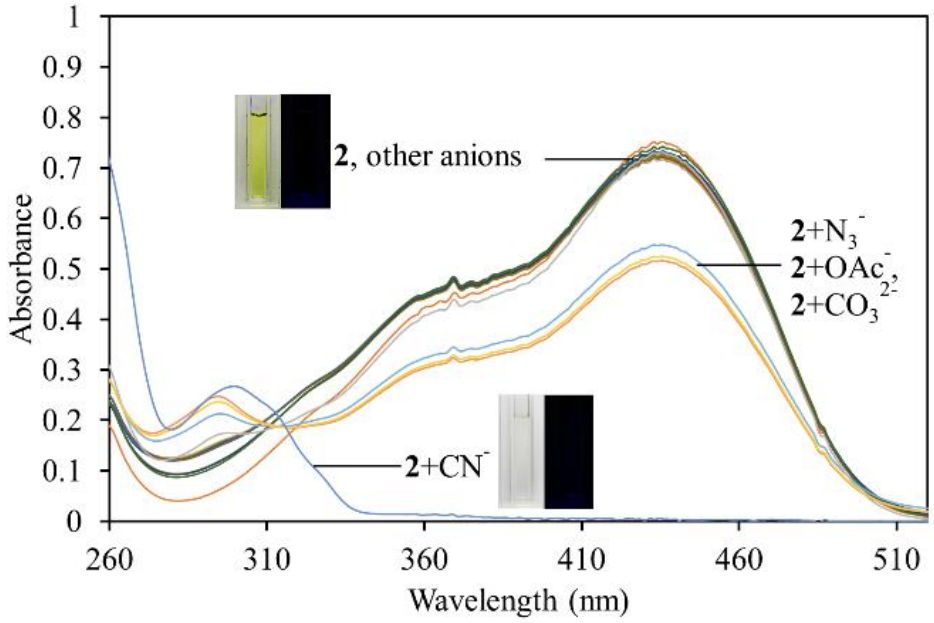

Figure 3.2 Absorption spectra of **2** (45 μM) in methanol solution upon addition of various anions (5 mM). Insets show the color of the solutions under room light and black light illuminations.

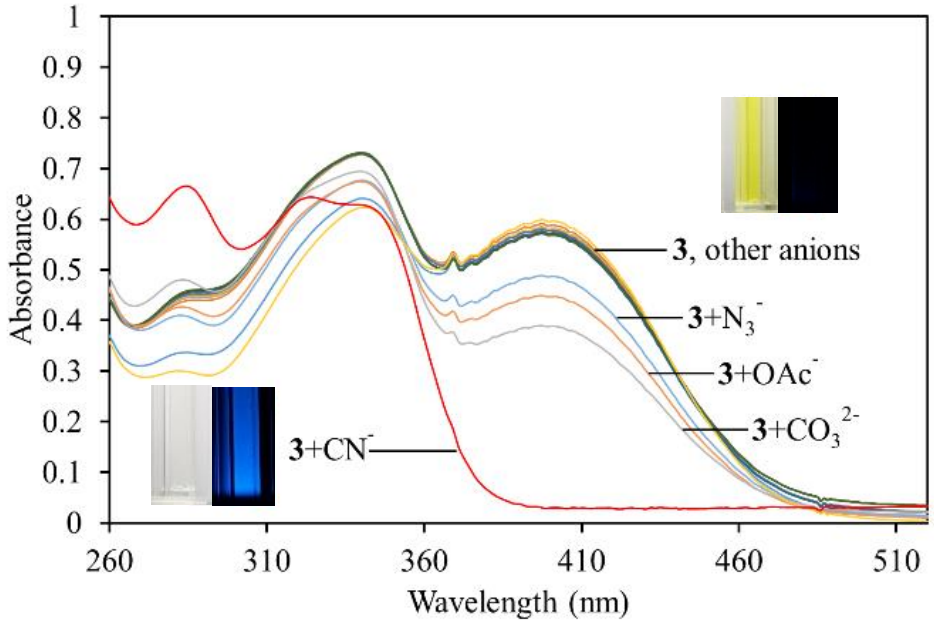

Figure 3.3 Absorption spectra of **3** (32 μM) in methanol solution upon addition of various anions (5 mM). Insets show the color of the solutions under room light and black light illuminations.

However, **1** did not show any response to the anion tested (Figure 3.4). This is reasonable considering that **1** was in the form of **1b** which contains no electrophilic

site. We could observe cyanide sensing activity of **1** at a much higher concentration of cyanide ion. The cyanide sensing activity of another spiropyran compound upon photoisomerization to the corresponding cyanine has been previously reported [35].

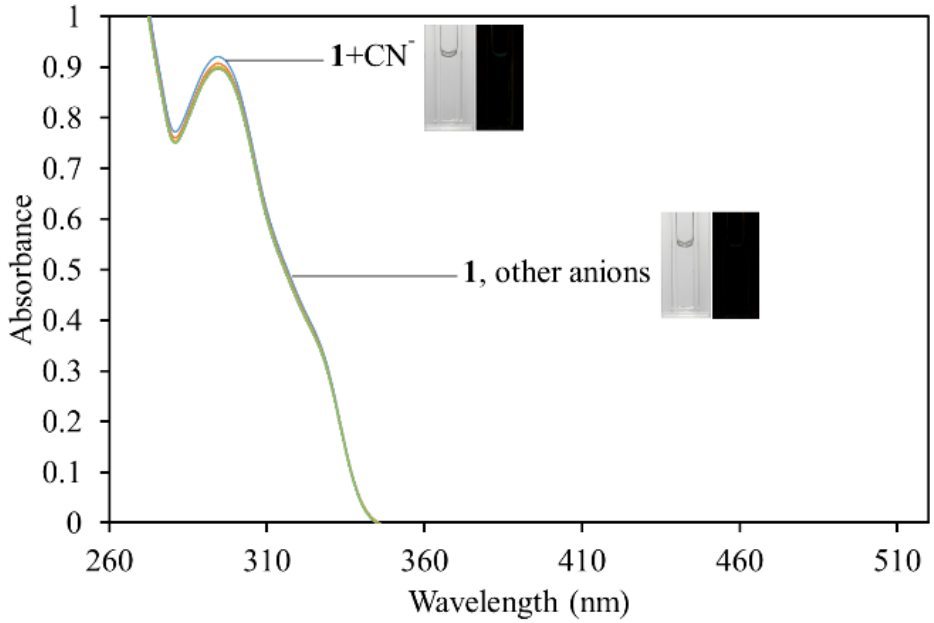

Figure 3.4 Absorption spectra of **1** (45 μM) in methanol solution upon addition of various anions (5 mM). Insets show the color of the solutions under room light and black light illuminations.

Under room light, the yellow solutions of **2** and **3** quickly turned colorless upon the addition of cyanide ion. Under black light illumination, the solution of **3** also showed strong blue fluorescence after the addition of cyanide, quantum efficiency of the solution improved from <0.01 to 0.40 at the excess of NaCN (10 equiv). While **2** did not give any observable fluorescence under the same treatment. The results suggested that **3** may be used as a dual modes of detection, both colorimetric and fluorometric, while **2** is only suitable for colorimetric sensing.

^{1}H NMR data indicated that both **2** and **3** underwent the same cyanide addition reaction. The reaction cleanly converted the iminium group to the aminonitrile group (Figure 3.5a). The mass spectroscopy also showed the formation of aminonitrile adducts of **2** and **3** (Figure A18-A19). The absence of observable fluorescence of the aminonitrile adduct of **2** was likely due to its short conjugation and the poor

fluorescence property of the styrene chromophore. The incorporation of aminophynylactetylene in compound **3** was thus proven to be effective for attaining visible emission. The fluorescence turn on signal is attributed to the conversion of the strong electron accepter iminium group to the more electron neutral aminonitrile group that critically relegate the ICT and PET fluorescence quenching processes.

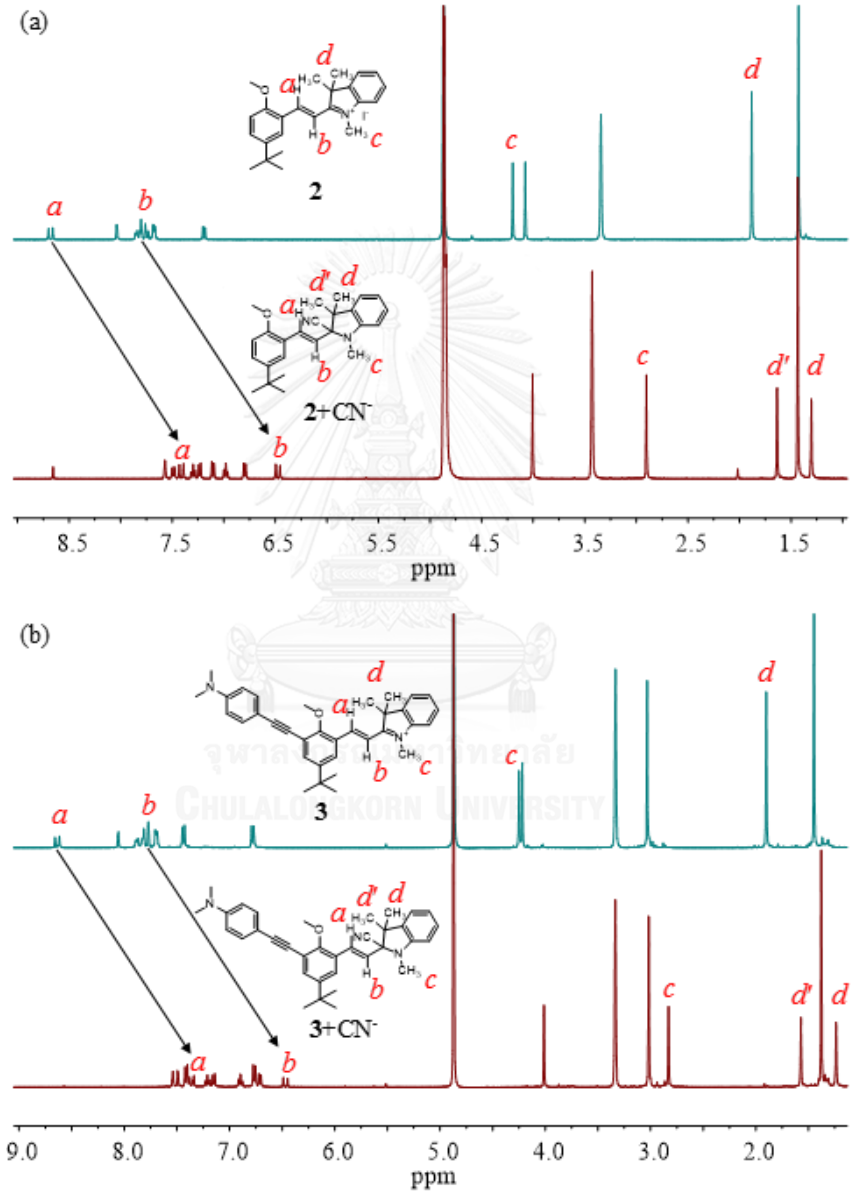

Figure 3.5 ^{1}H NMR spectra of (a) **2**, (b) **3** reacted with NaCN (1.2 equiv.) in CD_3OD.

3.4 Cyanide ion sensing in aqueous solution

Water is a primary medium of environmental and biological systems that responsible for trafficking of most cyanide contamination. It would thus be useful if the probes could be directly used for detection of cyanide ion in aqueous samples. For water soluble probe **2**, the determination of cyanide concentration was quick (Figure 3.6) and straight forward by measuring the UV-vis absorption of the solution in HEPES buffer pH 7.4 (Figure 3.7). This colorimetric method with probe **2** gave the detection limit of cyanide ion of 9.34 μM (Figure 3.8) which is somewhat higher than the WHO limit in drinking water (1.9 μM).

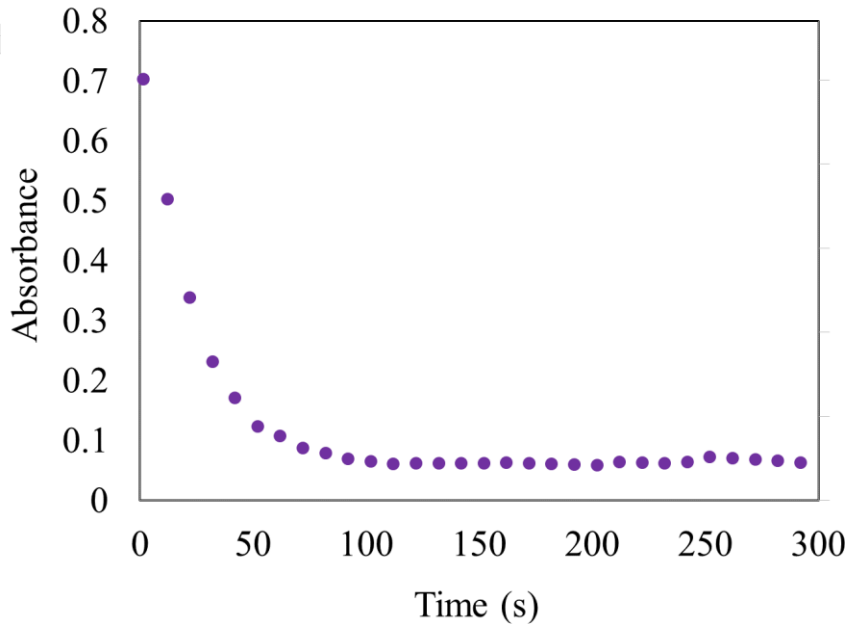

Figure 3.6 Time dependence of the absorbance of **3** in HEPES pH 6.0 with Triton X-100 (220 μM) after addition of NaCN (100 μM).

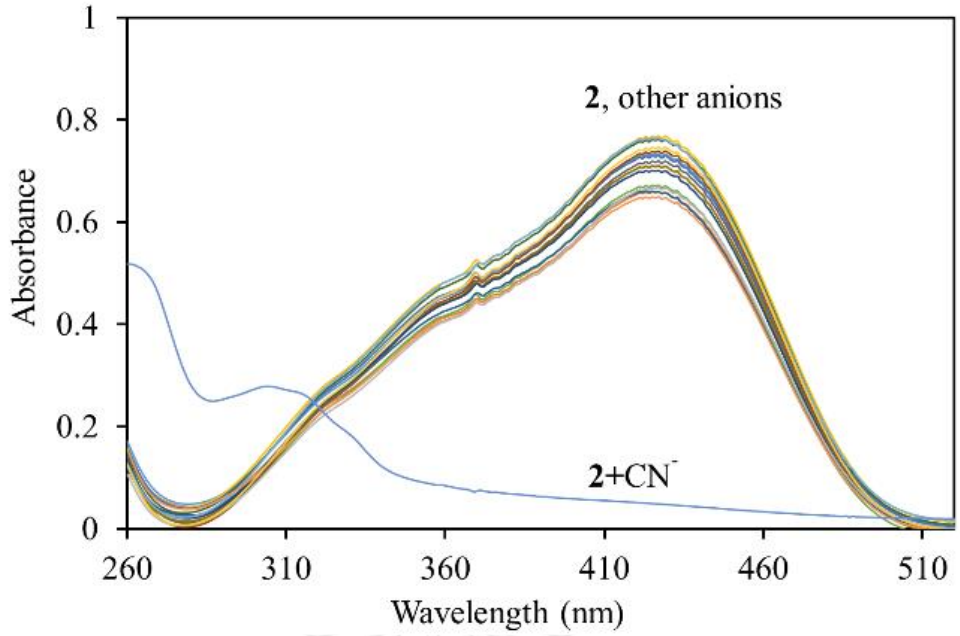

Figure 3.7 Absorption spectra of **2** (45 μM) upon addition of various anions in HEPES buffer pH 7.4.

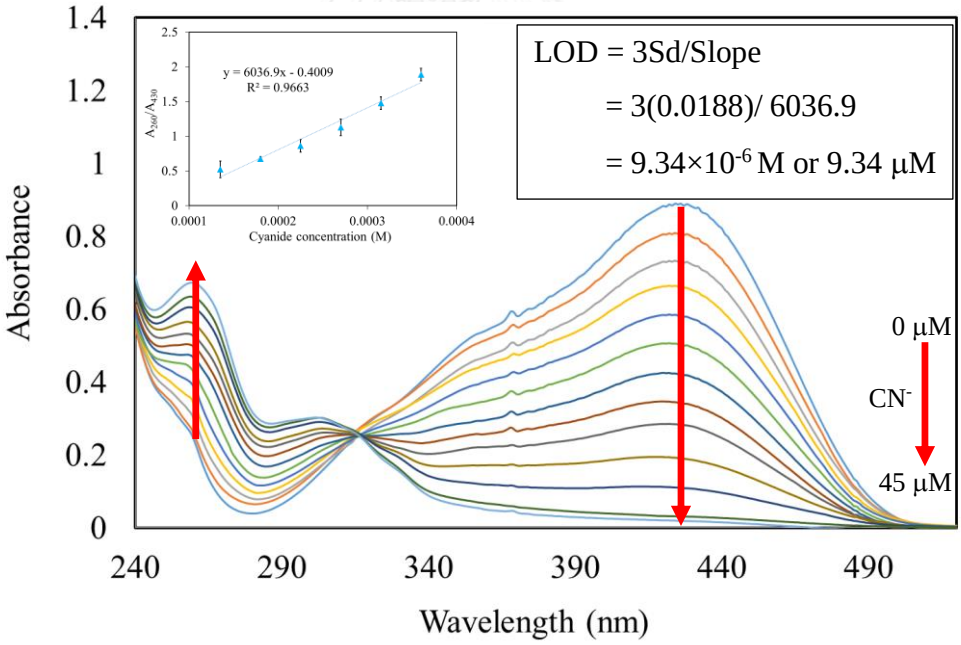

Figure 3.8 Colorimetric titration of **2** with cyanide ion and its absorption ratiometric plot.

Probe **3** is potentially more sensitive with the fluorometric method but its application in aqueous media was precluded as **3** is only sparingly soluble in water. Our initial test of compound **3** in CH_3CN/H_2O mixed solvent showed that the

fluorescence enhancement ratio dramatically dropped with the increase of water content (Figure 3.9).

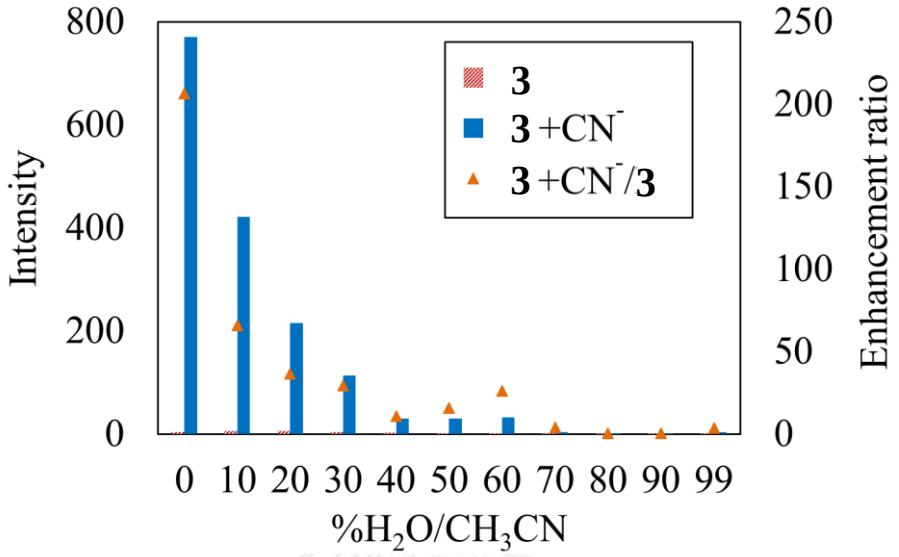

Figure 3.9 Fluorescence enhancement ratio of **3** (10 μM) in the presence of NaCN (100 μM) in CH_3CN/H_2O at various ratios.

This result suggested not only that the starting imidazolium salt **3** is poorly soluble in water but also that the fluorescent aminonitrile adduct is worse. We therefore adopted the utilization of micellar aqueous system, which has been previously used successfully in our various sensing systems. [43, 44] In aqueous solution, the fluorescence enhancement ratio of **3** upon the addition of NaCN increased with the concentration of a non-ionic surfactant Triton X-100. The fluorescence enhancement ratio increased with the concentration of Triton X-100 and became saturated near 40 times at the critical micelle concentration of Triton X-100 (220 μM) (Figure 3.10).

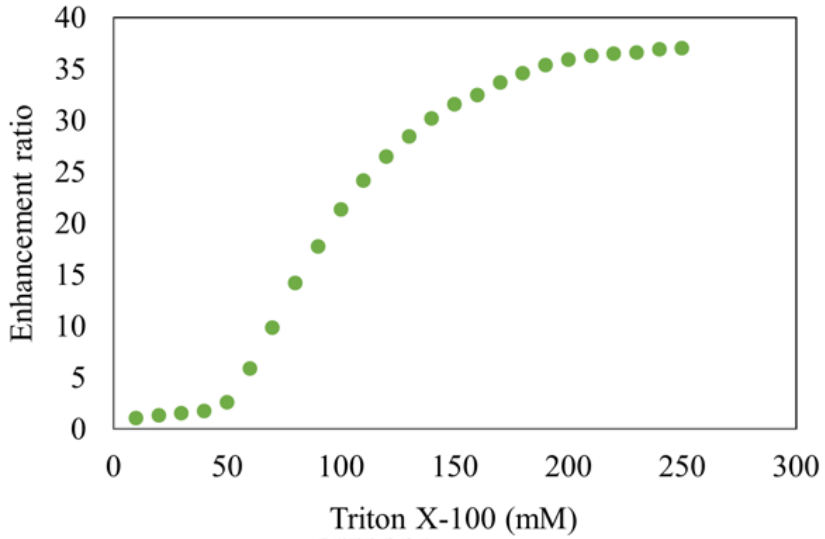

Figure 3.10 Fluorescence enhancement ratio of **3** (10 μM) in the presence of NaCN (100 μM) in aqueous solution containing various concentration of Triton X-100.

To further optimize the sensing conditions in aqueous media, the pH effect on cyanide sensing was studied. Acidic condition gave higher sensitivity of **3** toward cyanide ion (Figure 3.11). However, pH 6.0 was selected as a working pH to avoid the potential conversion of cyanide to hydrogen cyanide gas at the lower pH.

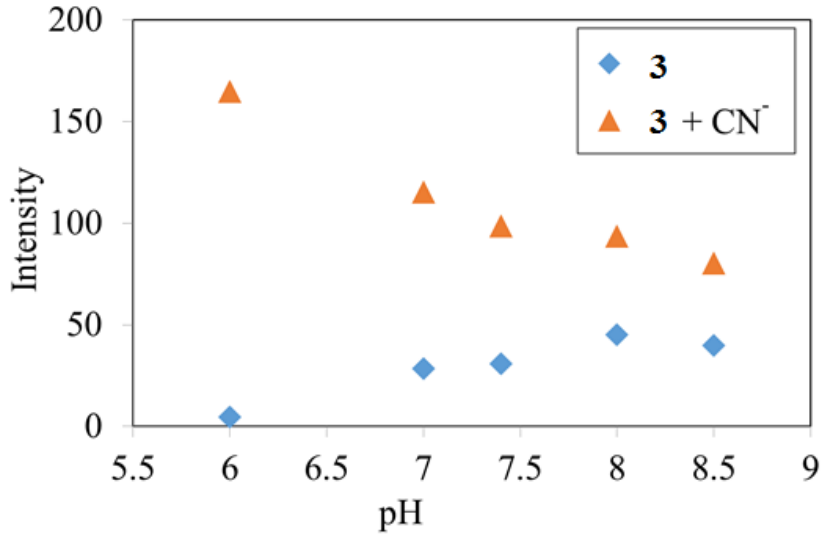

Figure 3.11 Fluorescence enhancement ratio after addition of NaCN (100 μM) to **3** (10 μM) in (a) aqueous solution containing Triton X-100 (220 μM) at various pH (10 mM HEPES buffer).

In aqueous HEPES buffer pH 6 solution containing Triton X-100, **3** showed slightly slower cyanide detection comparing with that in the methanol solution; ~95% of the maximum enhancement ratio was achieved in 2.5 minute in aqueous micellar solution comparing with 1 minute in methanol solution (Figure 3.12).

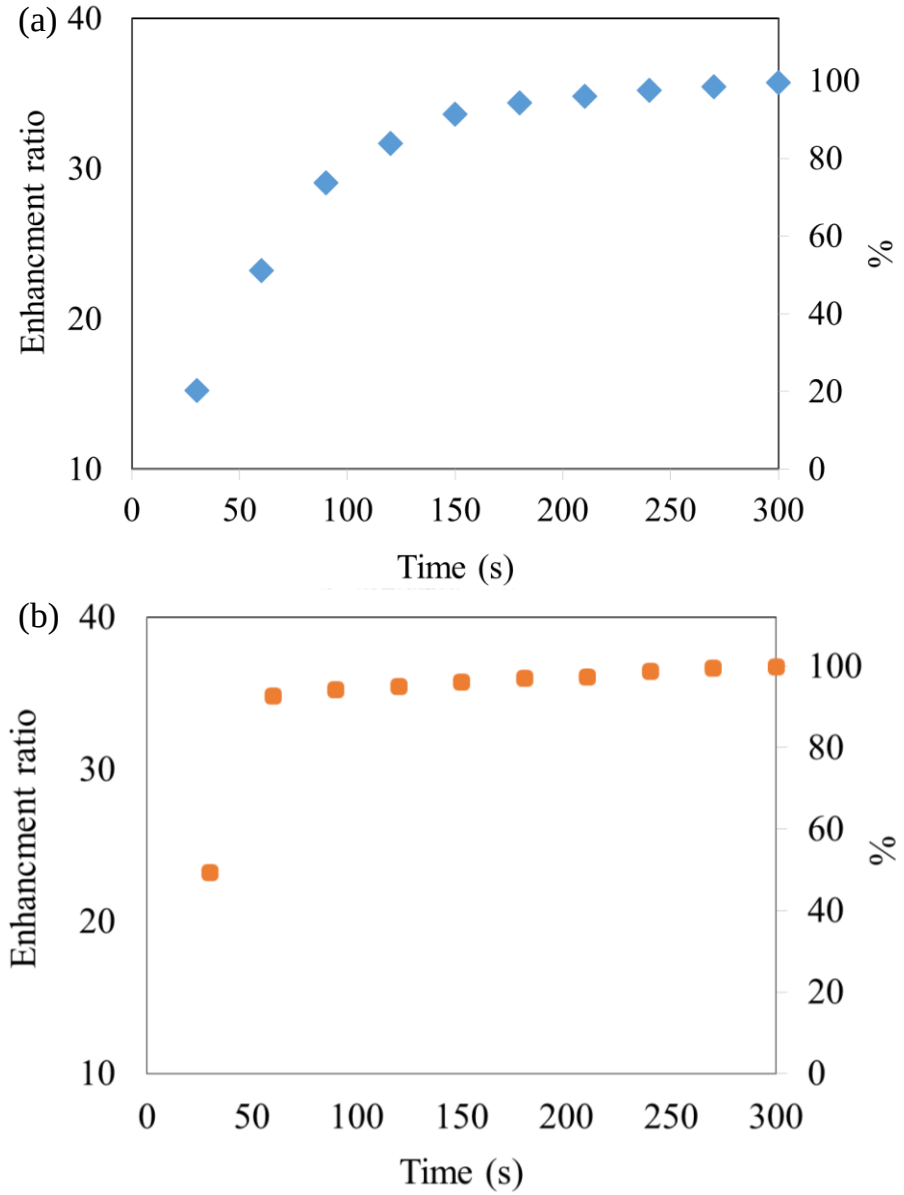

Figure 3.12 Fluorescence enhancement ratio after addition of NaCN (100 μM) to **3** (10 μM) in (a) HEPES pH 6.0 with Triton X-100 (220 μM) and (b) methanol.

In the aqueous solution, **3** however gave better selectivity comparing with that in methanol as there was no significant fluorescence responses to any other anions tested including acetate and azide ions. Probe **3** in the aqueous medium also showed

very low interference from other anions tested at the concentration 100 times of cyanide concentration (Figure 3.13).

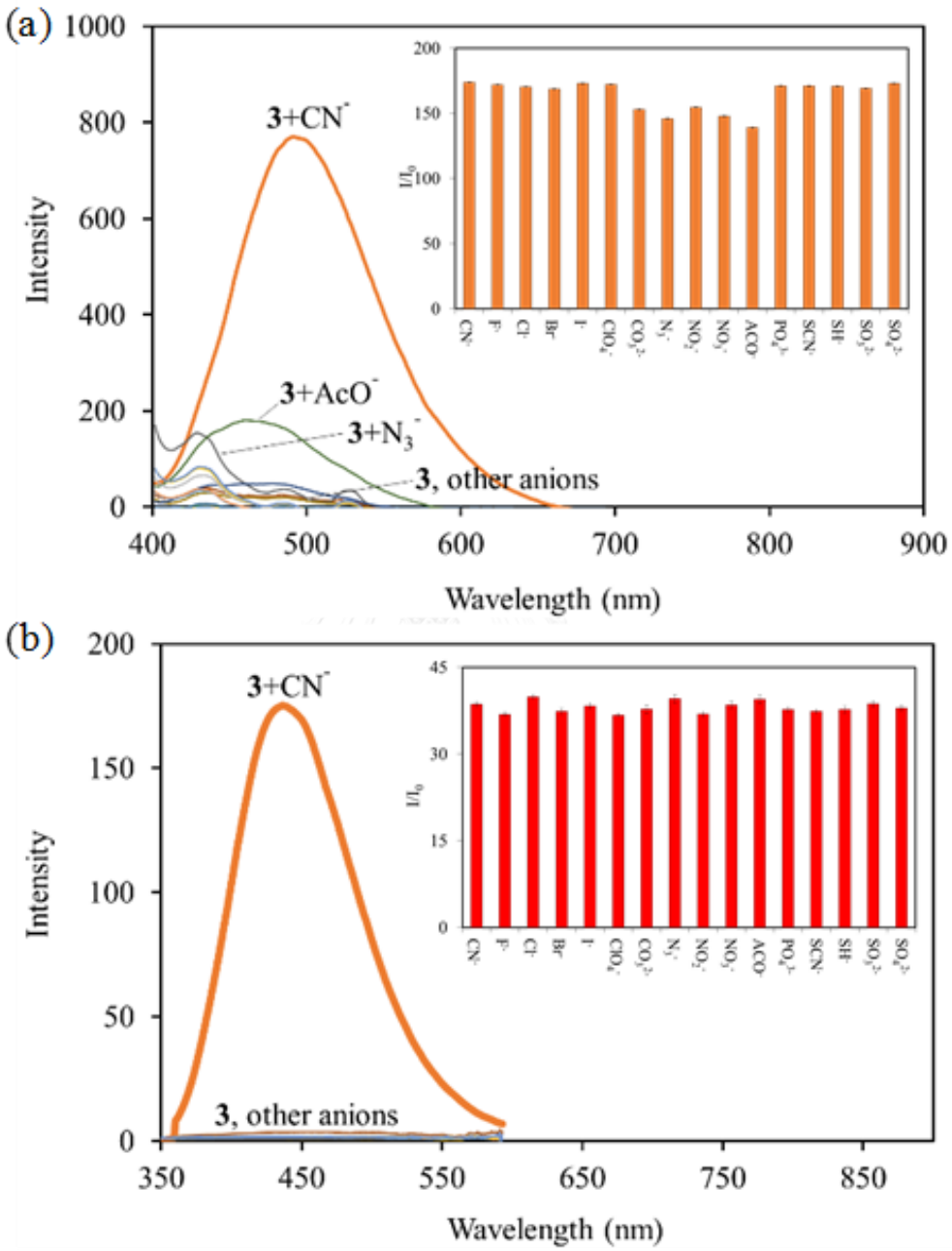

Figure 3.13 Fluorescence spectra of **3** (10 μM) upon addition of various anions (10 μM) in (a) methanol and (b) HEPES pH 6.0 buffer (10mM) with Triton X-100 (220 μM). Inset: fluorescence enhancement ratio (I/I_0) of **3** in the presence of cyanide ion (10 μM) and another ion (1.0 mM) tested for interference measured at λ_{em} (a) 490 nm and (b) 440 nm.

The colorimetric and fluorometric titration of **3** with cyanide ion were carried out in the optimized aqueous medium. The changes of the absorption and emission intensity linearly correlated with the concentration of cyanide ion with the limit of detection determined at 3 times of signal to noise ratio were 1.9 μM and 49 nM for the colorimetric (Figure 3.14) and fluorometric (Figure 3.15) methods, respectively.

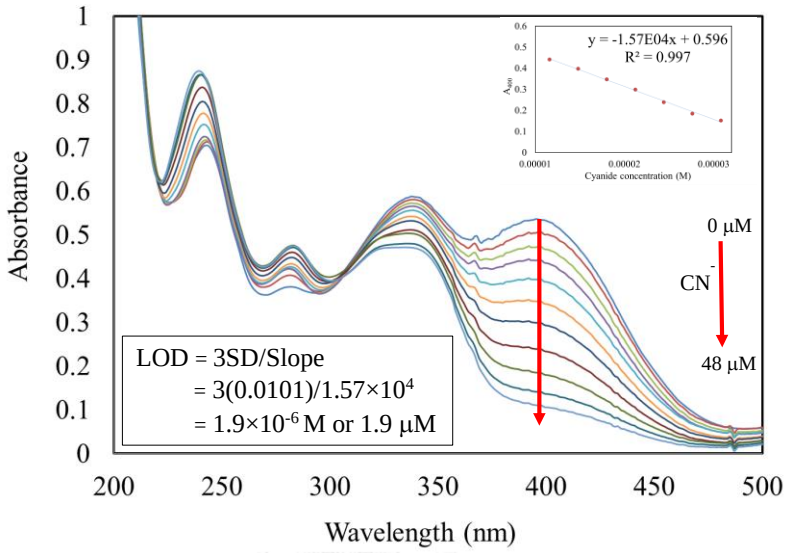

Figure 3.14 Absorption spectra of **3** (32 μM) upon titration with NaCN (0-48 μM) and its absorption intensity plot (inset).

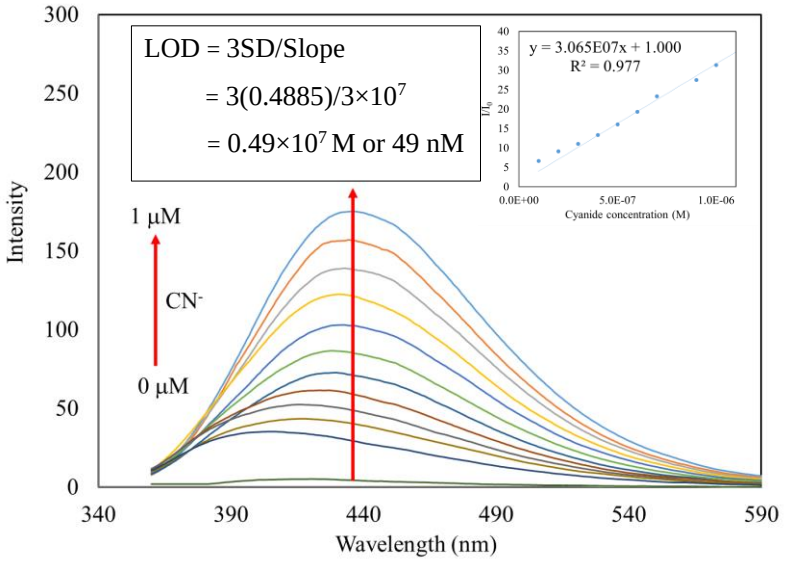

Figure 3.15 Fluorescence spectra of **3** (10 μM) upon titration with NaCN (0-12 μM) and its enhancement ratio plot (inset).

We found that sonication of the solutions after mixing the probe with cyanide significantly improved the sensitivity of the sensing system. The emission spectra of **3** showed sharp increase of the fluorescence intensity even at nanomolar level of NaCN (Figure 3.16). The fluorescence enhancement ratio (I/I_0) increased linearly with the concentration of NaCN in the range of 0-8 nM giving the detection limit of 0.54 nM, a remarkable 100 times improvement from the non-sonication method.

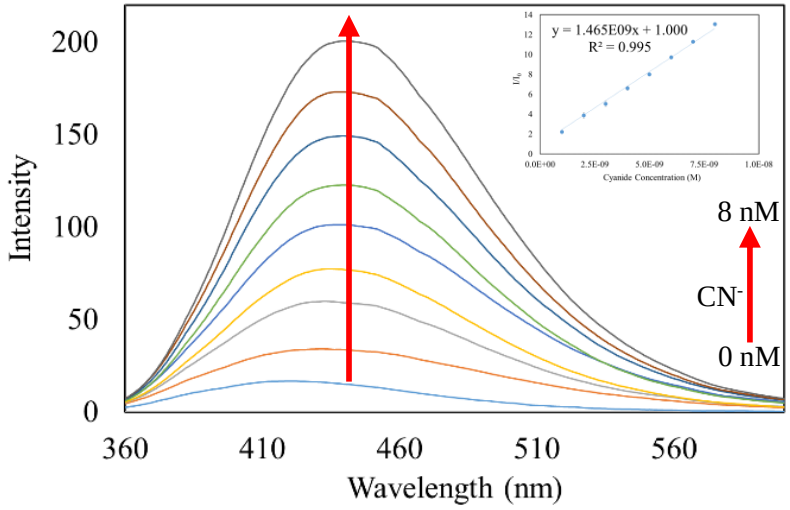

Figure 3.16 Fluorescence spectra of sonicated solution of **3** (10 μM) upon titration with NaCN (0-8 μM) in HEPES buffer pH 6.0 with Triton X-100 (220 μM) and its enhancement ratio plot (inset).

This is by far the most sensitive fluorescent sensors for cyanide in aqueous solution (Table 3.2). We postulate that the sonication improved the sensitivity of probe **3** in aqueous micellar system by increasing the rate of micellar self-assembly dynamic process allowing a faster reaction between cyanide ion and the probe.

Table 3.2 Comparison of CN^- detection limit of **3** with other reported.

Receptors	Sensing modes	Solvents	LOD (nM)	Ref.
imidazolium	Turn-off fluorescence	95% EtOH in PBS buffer pH 7.4	500	[45]
indolium	Turn-on fluorescence	HEPES buffer pH 7.4 with α-cyclodrextin (400 μM)	1300	[46]
bisimidazole	Turn-on fluorescence	10% DMSO in H_2O	1040	[47]
benzothiazol	Turn-off fluorescence	60% DMSO in HEPES buffer pH 7.26	180	[48]
pillar[5]arene	Turn-on fluorescence	80% DMSO in H_2O	10.8	[49]
benzothiazol	Absoprtion	50% DMSO in HEPES buffer pH 7.2	280	[50]
salicylaldehyde	Turn-on fluorescence	90% DMSO in Tris-HCl buffer pH 7.4	880	[51]
3	Turn-on fluorescence	HEPES buffer pH 6.0 with Triton X-100 (220 μM)	0.54	This work

With very high sensitivity and selectivity of our developed sensing system, its application for naked eye detection of cyanide ion in water was imminent. The naked eye detection was tested at 100 μM of **3**, a 10 times higher than the concentration used in the fluorescence measurement by the spectrometer. Although the observation under room light showed color fading in 10s micromolar levels of NaCN, the observation under black light illumination showed blue fluorescence in submicromolar level of cyanide ion (Figure 3.17). The results demonstrate that our optimized sensing system can be used for naked eye detection of cyanide ion in water at the concentration well below the WHO limit given for cyanide concentration in drinking water (1.9 μM).

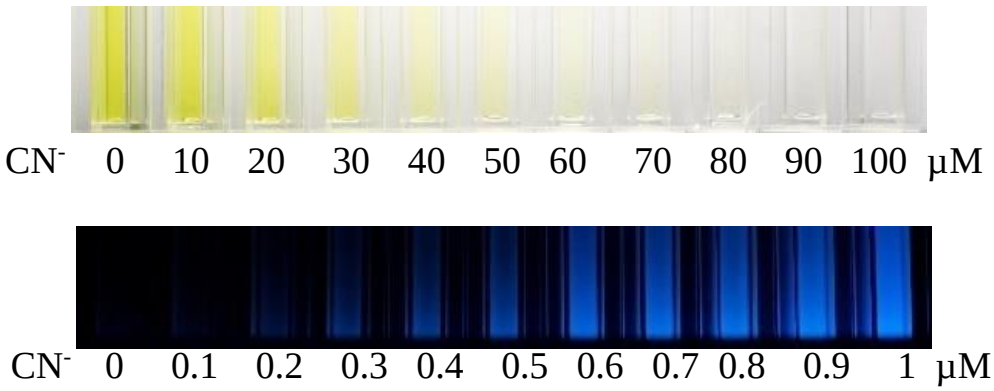

Figure 3.17 Photographs of **3** (100 µM) with various concentration of NaCN under room light (top) and black light (bottom) illuminations. All solutions were sonicated for 30 min before being measured and photographed.

3.5 Cyanide sensing on filter paper and in alginate gel bead

Litmus type indicator for cyanide sensing was developed by deposit **3** on wax-printed filter paper strip. The indicator still gave high selectivity toward cyanide ion for both color and fluorescence observation (Figure 3.18). Naked eye detection of this paper-based indicator was possible with 150 pg of cyanide per mm^2 of the detection area that used 2 µL of 30 µM NaCN.

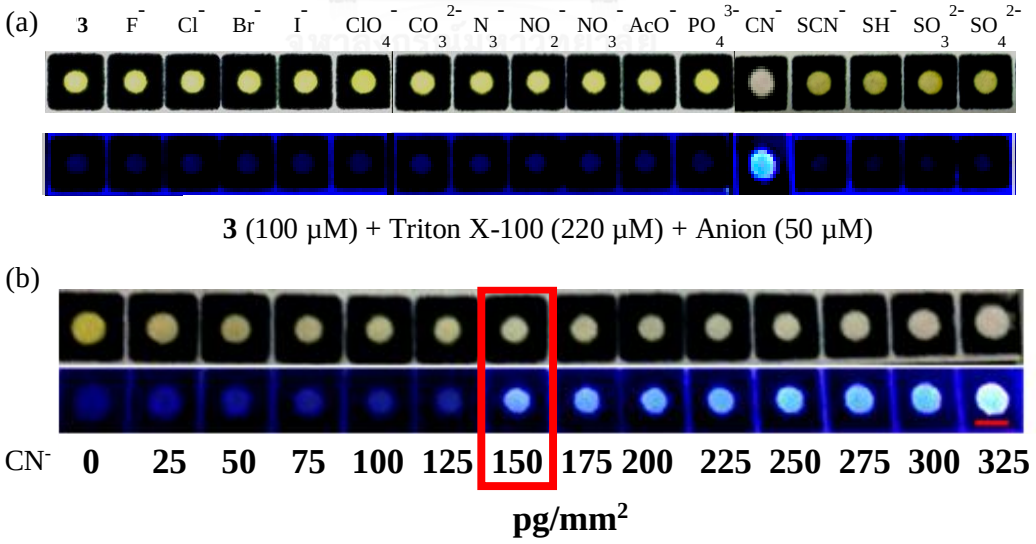

Figure 3.18 Images of (a) paper-based sensor made of **3** tested with various anion, (b) amount of NaCN under room light and black light illuminations (Scale bar 5 mm).

This type of indicator is thus suitable of small sample volume but the detectable concentration is significantly higher than that in solution. The small volume used for this detection of the paper surface also provided another benefit to lower interference from colored samples, such as red wine, grape and orange juices (Figure 3.19).

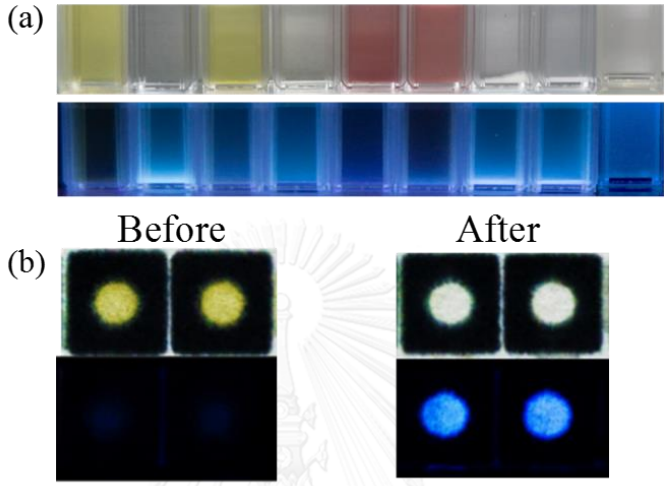

Figure 3.19 Images under room light and black light of (a) spiked sample solution after added **3** to various medias; control, drinking water, orange juice, apple juice, grape juice, red wine, Tylenol with drinking water, starch with drinking water and sea water, respectively and (b) paper-based sensor made of **3** before and after tested with grape juice and red wine which was spiked NaCN (1 mM).

Due to its hydrophilicity and high water permeability, alginate gel bead was tested as another solid medium for cyanide sensing with probe **3** in order to improve the sensitivity for naked eye detection of cyanide ion in solid medium. The normal gel beads, prepared by dropping the alginate solution containing **3** into $CaCl_2$ coagulating solution, showed poor sensitivity that the blue fluorescence became detectable with NaCN concentration greater than 100 μM (Figure 3.20)

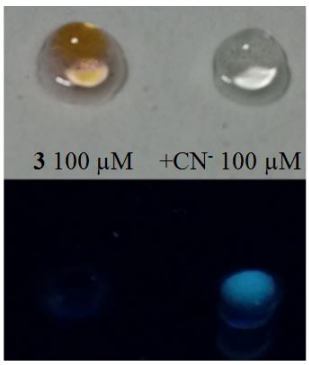

Figure 3.20 Pictures of normal alginate beads with **3** and **3**+CN^- under room light and black light.

The reverse gel beads, prepared by dropping $CaCl_2$ coagulating solution containing **3** into the alginate solution, however showed blue fluorescence observable under black light illumination with only 1 μM of NaCN (Figure 3.21). This level of sensitivity of the sensing bead is also below the WHO cyanide limit for drinking water (1.9 μM). The higher sensitivity of the reverse gel bead comparing to the normal gel bead is probably attributed to that the crosslinking reaction between calcium ion and alginate is limited at the surface leaving the sensing solution inside. To the best of our knowledge, this is the first demonstration of reverse coagulation used for improving sensitivity of solid-state optical sensors. The beads offer convenient applications for on-site detection and low sample volume required similar to that of that of paper-based indicator but higher sensitivity.

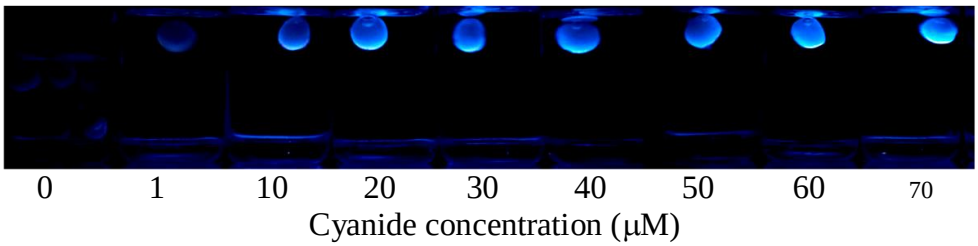

Figure 3.21 Images of reverse spherification bead sensors with various concentration of NaCN under room light and black light illuminations.

CHAPTER IV
CONCLUSIONS

Novel π-conjugated indolium salts (**1**, **2** and **3**) were synthesized and evaluated for cyanide turn-on fluorescence sensing. Compound **3** containing extended π-conjugated system in cyanine form showed a strong fluorescence enhancement upon the addition reaction with cyanide. The cyanide sensitivity of **3** in water was much lower than in methanol due to the low water solubility of both probe and the aminitrile adduct. The cyanide sensitivity in aqueous media could be vastly improved in micellar system of Triton X-100. The limit of fluorescence detection of cyanide ion with **3** in the aqueous micellar system using sonication mixing was as low as 0.54 nM which is one of the best to date. Paper-based and gel-based indicators for naked eye detection of cyanide ion were also developed. The alginate gel beads containing probe **3**, prepared by reverse coagulating method, showed remarkable sensitivity for naked eye detection of cyanide as low as 1 μM.

REFERENCES

[1] Bett, S. The Jablonski diagram. 2014.

[2] Lakowicz, J.R. Principles of fluorescence spectroscopy. 3rd ed. New York: Springer, 2006.

[3] Niamnont, N. Synthesis and Fluorescent Properties of Dendritic Polyelectrolyte Fluorophores. Doctoral Degree, Chulalongkorn University, 2010.

[4] Druzhinin, S.I., et al. Intramolecular Charge Transfer with 1-tert-Butyl-6-cyano-1,2,3,4-tetrahydroquinoline (NTC6) and Other Aminobenzonitriles. A Comparison of Experimental Vapor Phase Spectra and Crystal Structures with Calculations. Journal of the American Chemical Society, 132, (2010): 7730-7744.

[5] Galievsky, V.A., et al. Ultrafast Intramolecular Charge Transfer with N-(4-Cyanophenyl)carbazole. Evidence for a LE Precursor and Dual LE + ICT Fluorescence. The Journal of Physical Chemistry A, 114, (2010): 12622-12638.

[6] Chung, S.K., et al. A Selective Colorimetric Hg^{2+} Probe Featuring a Styryl Dithiaazacrown Containing Platinum(II) Terpyridine Complex through Modulation of the Relative Strength of ICT and MLCT Transitions. Inorganic Chemistry, 50, (2011): 2711-2713.

[7] Henary, M.M. and Fahrni, C.J. Excited State Intramolecular Proton Transfer and Metal Ion Complexation of 2-(2‘-Hydroxyphenyl)benzazoles in Aqueous Solution. The Journal of Physical Chemistry A, 106(21) (2002): 5210-5220.

[8] Gunnlaugsson, T., et al. Dual Responsive Chemosensors for Anions: The Combination of Fluorescent PET (Photoinduced Electron Transfer) and Colorimetric Chemosensors in a Single Molecule. Tetrahedron Letters, 44, (2003): 6575-6578.

[9] Hu, R., et al. A Rapid Aqueous Fluoride Ion Sensor with Dual Output Modes. Angewandte Chemie International Edition, 49, (2010): 4915-4918.

[10] Sun, Y.Q., et al. A Fluorescent Turn-on Probe for Bisulfite Based on Hydrogen Bond-inhibited C=N Isomerization Mechanism. Analyst, 137, (2012): 3430-3433.

[11] Ma, X., et al. A fluorescein-based probe with high selectivity and sensitivity for sulfite detection in aqueous solution. Sensors and Actuators B: Chemical, 188, (2013): 1196-1200.

[12] Egli, M., Saenger, W., Principles of Nucleic Acid Structure. New York: Springer, 1984.

[13] Adams, R.L.P., et al. The Biochemistry of the Nucleic Acids. Springer Netherlands, 1986.

[14] Bazzicalupi, C., et al. ATP Recognition and Sensing with a Phenanthroline-containing Polyammonium Receptor. Chemical Communications, 39, (2006): 4087-4089.

[15] Kurishita, Y., et al. Rational Design of FRET-Based Ratiometric Chemosensors for in Vitro and in Cell Fluorescence Analyses of Nucleoside Polyphosphates. Journal of the American Chemical Society, 132, (2010): 13290-13299.

[16] Isom, G.E. and Way, J.L. Effect of Oxygen on Cyanide Intoxication. VI. Reactivation of Cyanide-inhibited Glucose Metabolism. The Journal of pharmacology and experimental therapeutics, 189, (1974): 235-243.

[17] Young, C. Cyanide : social, industrial, and economic aspects. Minerals, Metals & Materials Society, 2001

[18] Jones, D.A. Why are so Many Food Plants Cyanogenic? Phytochemistry, 47, (1998): 155-162.

[19] Greenfield, R.A., et al. Microbiological, Biological, and Chemical Weapons of Warfare and Terrorism. American Journal of the Medical Sciences, 323, (2002): 326-40.

[20] W.H.O., W.H.O. Guidelines for Drinking-water Quality: Recommendations. Vol. 1: World Health Organization, 2004.

[21] Garcia, F., et al. Pyrylium-containing Polymers as Sensory Materials for the Colorimetric Sensing of Cyanide in Water. Chemical Communications, 22, (2005): 2790-2792.

[22] Pati, P.B. and Zade, S.S. Dicyanovinyl Terthiophene as a Reaction Based Colorimetric and Ratiometric Fluorescence Probe for Cyanide Anions. Rsc Advances, 3, (2013): 13457-13462.

[23] Niamnont, N., et al. Novel Salicylaldehyde Derivatives as Fluorescence Turn-on Sensors for Cyanide Ion. Journal of Hazardous Materials, 280, (2014): 458-463.

[24] Andruch, V., et al. Investigation of 2-[2-(4-methoxy-phenylamino)-vinyl]-1,3,3-trimethyl-3H-indolium Chloride as a new Reagent for the Determination of Chromium(VI). Microchimica Acta, 142, (2003): 109-113.

[25] Balogh, I.S., et al. Spectrophotometric Determination of Manganese with Derivatives of 1,3,3-trimethyl-2-[3-(1,3,3-trimethyl-1,3- H-indol-2-ylidene)propenyl]-3 H-indolium. Analytical and Bioanalytical Chemistry, 377, (2003): 709-714.

[26] Balogh, I.S., at al. An Investigation of the Reaction of Copper Ions with Dimethylindodicarbocyanine Dye: An Application for the Determination of Cu(I), Cu(II) and Cu(III). Talanta, 76, (2008): 111-115.

[27] Leskova, M., et al. A Non-extractive Sequential Injection Method for Determination of Molybdenum. Talanta, 96, (2012): 185-189.

[28] Kocúrová, L., at al. Dispersive Liquid-phase Microextraction Procedure for Spectrometric Determination of Cadmium. Microchemical Journal, 107, (2013): 3-9.

[29] Li, J., et al. Ratiometric Fluorescent Probes for ClO^- and in Vivo Applications. Dyes and Pigments, 130, (2016): 209-215.

[30] Hong, S.J., et al. Beta-vinyl Substituted Calix[4]pyrrole as a Selective Ratiometric Sensor for Cyanide Anion. Chemical Communications, 2, (2009): 189-191.

[31] Lee, J.H., et al. Fluorescence Turn-on Sensor for Cyanide Based on a Cobalt(II)-Coumarinylsalen Complex. Organic Letters, 12, (2010): 764-767.

[32] Zhan, X.Q., et al. Sensing Hydrogen Peroxide Involving Intramolecular Charge Transfer Pathway: A Boronate-functioned Styryl Dye as a Highly Selective and Sensitive Naked-eye Sensor. Analytica Chimica Acta, 658, (2010): 175-179.

[33] Li, Y., et al. Selective Tracking of Lysosomal Cu^{2+} Ions Using Simultaneous Target- and Location-activated Fluorescent Nanoprobes. Analytical Chemistry 87(1) (2015): 584-591.

[34] Wu, Y., et al. Pyrene Derivative Emitting Red or Near-Infrared Light with Monomer/Excimer Conversion and Its Application to Ratiometric Detection of Hypochlorite. ACS Applied Materials & Interfaces, 8, (2016): 1511-1519.

[35] Shiraishi, Y., et al. Highly sensitive cyanide anion detection with a coumarin-spiropyran conjugate as a fluorescent receptor. Chemical Communications, 47, (2011): 4953-4955.

[36] Lv, X., et al. Ratiometric Fluorescence Detection of Cyanide Based on a Hybrid Coumarin-hemicyanine Dye: the Large Emission Shift and the High Selectivity. Chemical Communications, 47, (2011): 12843-12845.

[37] Shiraishi, Y., et al. Rapid, Selective, and Sensitive Fluorometric Detection of Cyanide Anions in Aqueous Media by Cyanine Dyes with Indolium-coumarin Linkages. Chemical Communications, 50, (2014): 11583-11586.

[38] Peng, M.J., et al. Coumarin-hemicyanine Conjugates as Novel Reaction-based Sensors for Cyanide Detection: Convenient Synthesis and ICT Mechanism. RSC Advances, 4, (2014): 19077-19085.

[39] Zhou, C., et al. A New Colorimetric and Fluorescent Chemodosimeter for Fast Detection of Cyanide. Sensors and Actuators B: Chemical, 203, (2014): 382-387.

[40] Wang, S., et al. A Triphenylamine-based Colorimetric and "Turn-on" Fluorescent Probe for Detection of Cyanide Anions in Live Cells. RSC Advances, 5, (2015): 47990-47996.

[41] Wang, S., et al. A Novel Reaction-based Colorimetric and Ratiometric Fluorescent Sensor for Cyanide Anion with a Large Emission Shift and High Selectivity. Talanta, 148, (2016): 229-236.

[42] Chao, J., et al. A Ratiometric Fluorescence Probe for Monitoring Cyanide Ion in Live Cells. Sensors and Actuators B: Chemical, 228, (2016): 192-199.

[43] Niamnont, N., et al. A Polyanionic Dendritic Fluorophore for Selective Detection of Hg^{2+} in Triton X-100 Aqueous Media. Organic Letters, 11, (2009): 2768-2771.

[44] Niamnont, N., et al. Novel Salicylaldehyde Derivatives as Fluorescence Turn-on Sensors for Cyanide Ion. Journal of Hazardous Materials, 280, (2014): 458-463.

[45] Kumar, A. and Kim, H.S. A Pyrenesulfonyl-imidazolium Derivative as a Selective Cyanide Ion Sensor in Aqueous Media. New Journal of Chemistry, 39, (2015): 2935-2942.

[46] Niamnont, N., et al. A Novel Phenylacetylene-indolium Fluorophore for Detection of Cyanide by the Naked Eye. RSC Advances, 5, (2015): 64763-64768.

[47] Mardanya, S., et al. An Imidazolyl-pyreno-imidazole Conjugate as a Cyanide Sensor and a Set-reset Memorized Sequential Logic Device. Dalton Transactions, 44, (2015): 15994-16012.

[48] Li, J., et al. A “Donor-two-acceptor” Sensor for Cyanide Detection in Aqueous Solution. Sensors and Actuators B: Chemical, 220, (2015): 986-991.

[49] Cheng, X., et al. A Pillar[5]arene-based Cyanide Sensor Bearing on a Novel Cyanide-induced Self-assemble Mechanism. Dyes and Pigments, 127, (2016): 59-66.

[50] Li, J., et al. Highly Selective Colorimetric/Fluorometric Dual-channel Sensor for Cyanide Based on ICT Off in Aqueous Solution. Sensors and Actuators B: Chemical, 228, (2016): 330-334.

[51] Sukato, R., et al. New Turn-on Fluorescent and Colorimetric Probe for Cyanide Detection Based on BODIPY-salicylaldehyde and Its Application in Cell Imaging. Journal of Hazardous Materials, 314, (2016): 277-285.

APPENDIX

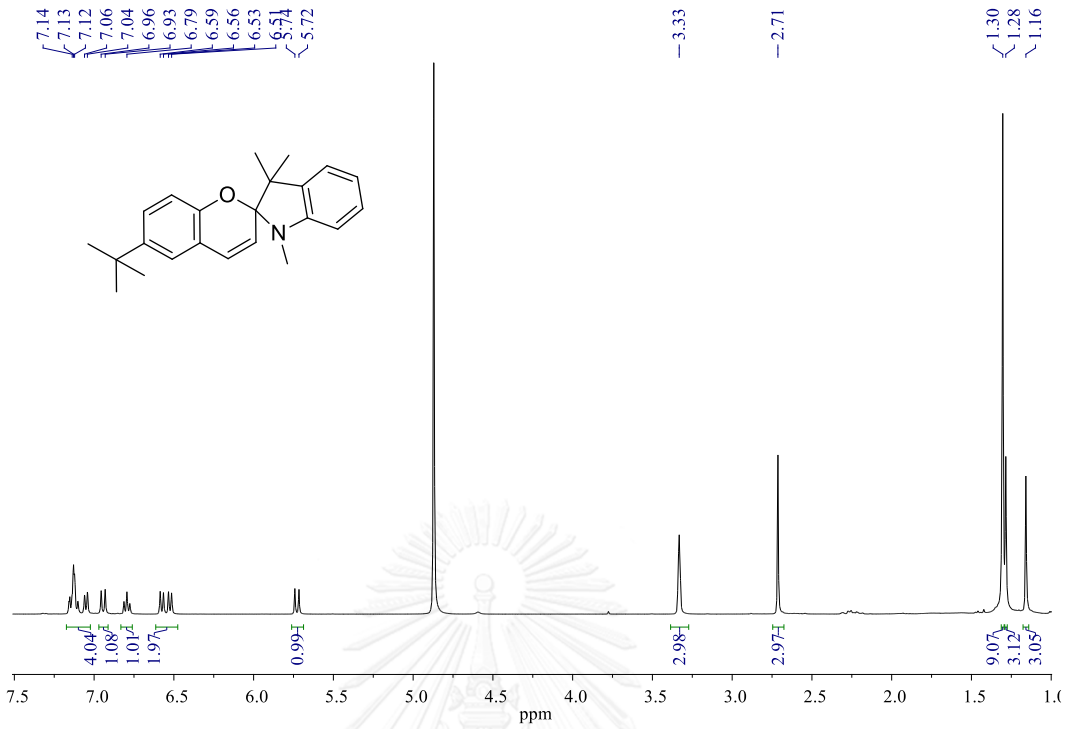

Figure A1 ^{1}H NMR spectrum of compound **1b** in CD_3OD.

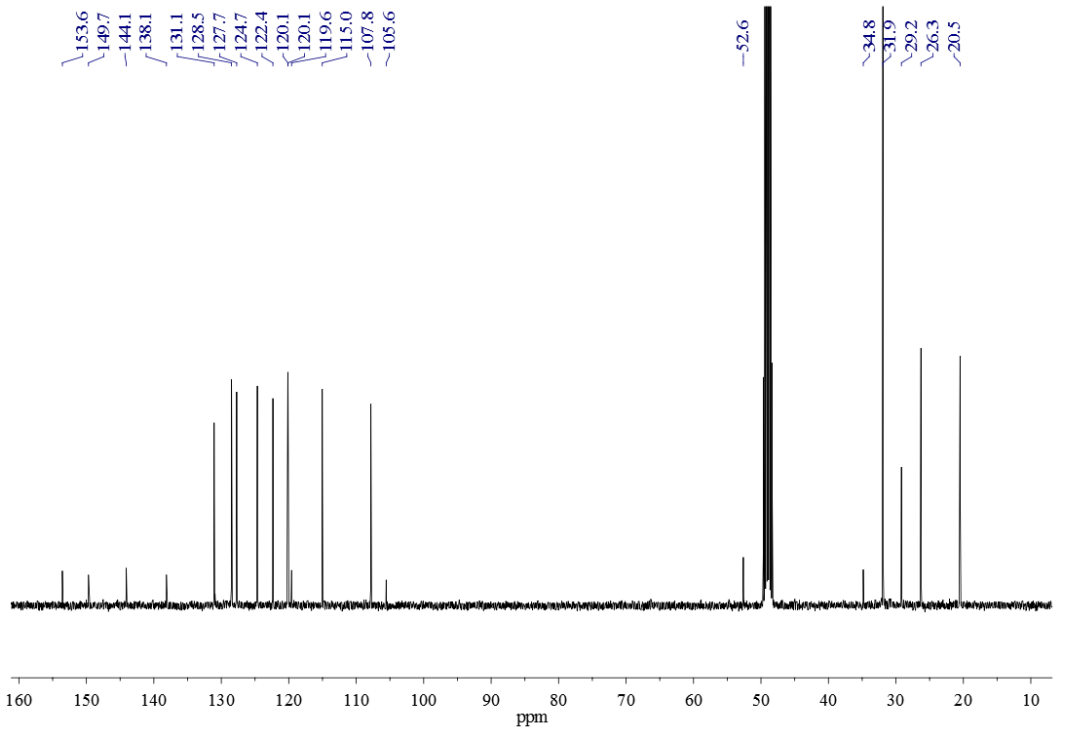

Figure A2 ^{13}C NMR spectrum of compound **1b** in CD_3OD.

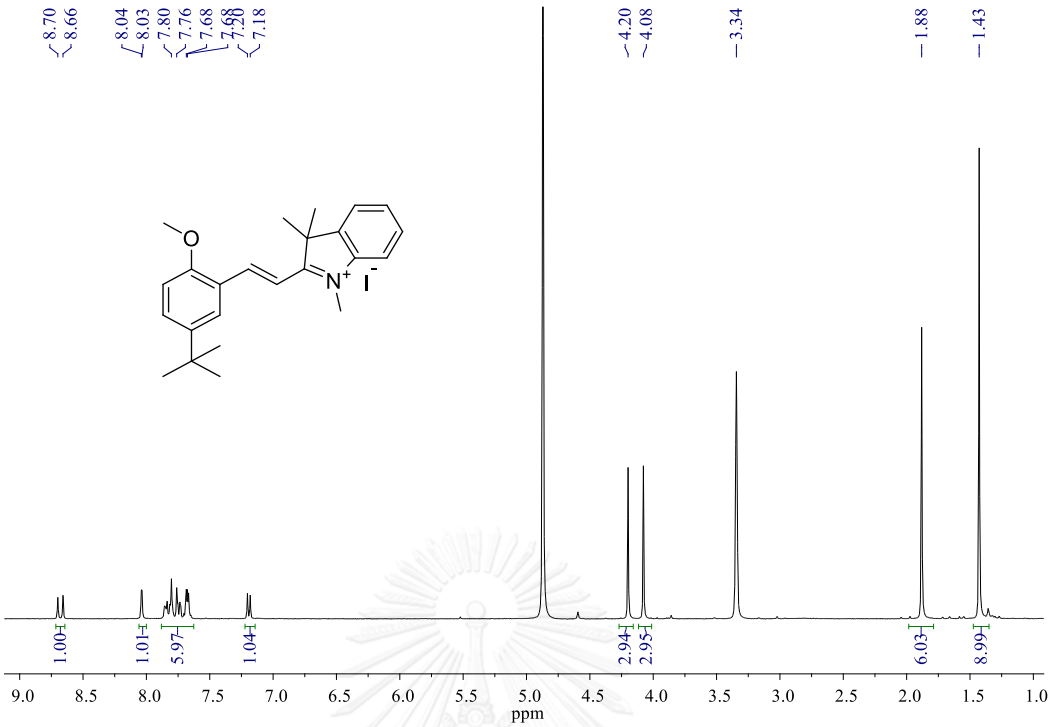

Figure A3 ^{1}H NMR spectrum of compound **2** in CD_3OD.

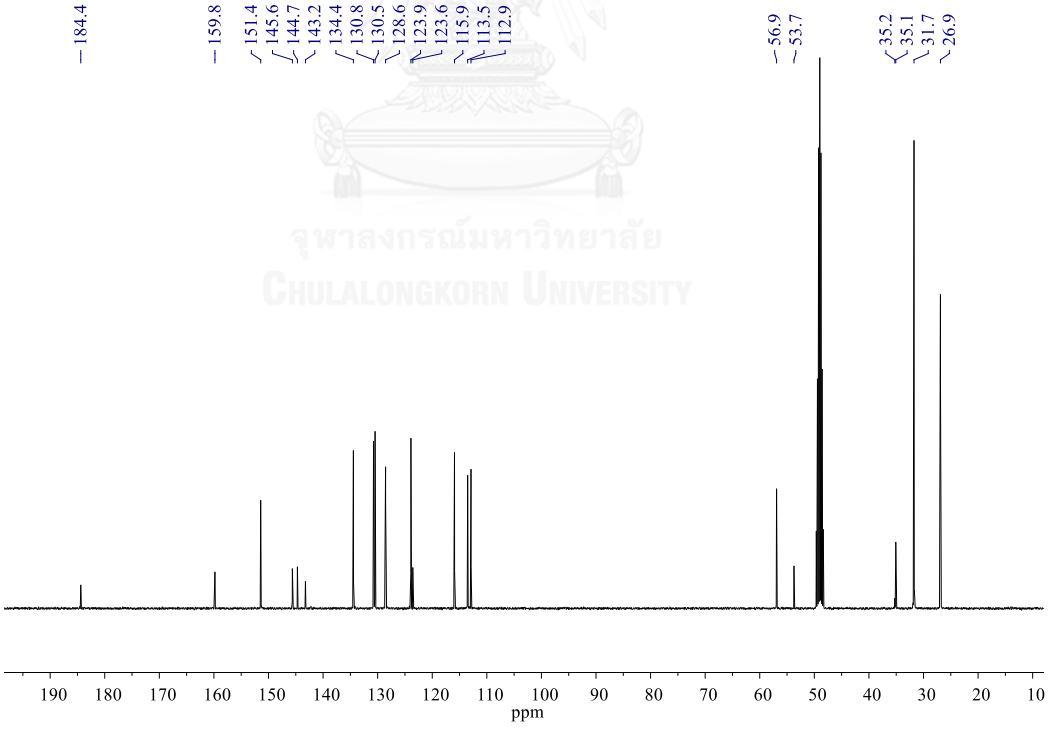

Figure A4 ^{13}C NMR spectrum of compound **2** in CD_3OD.

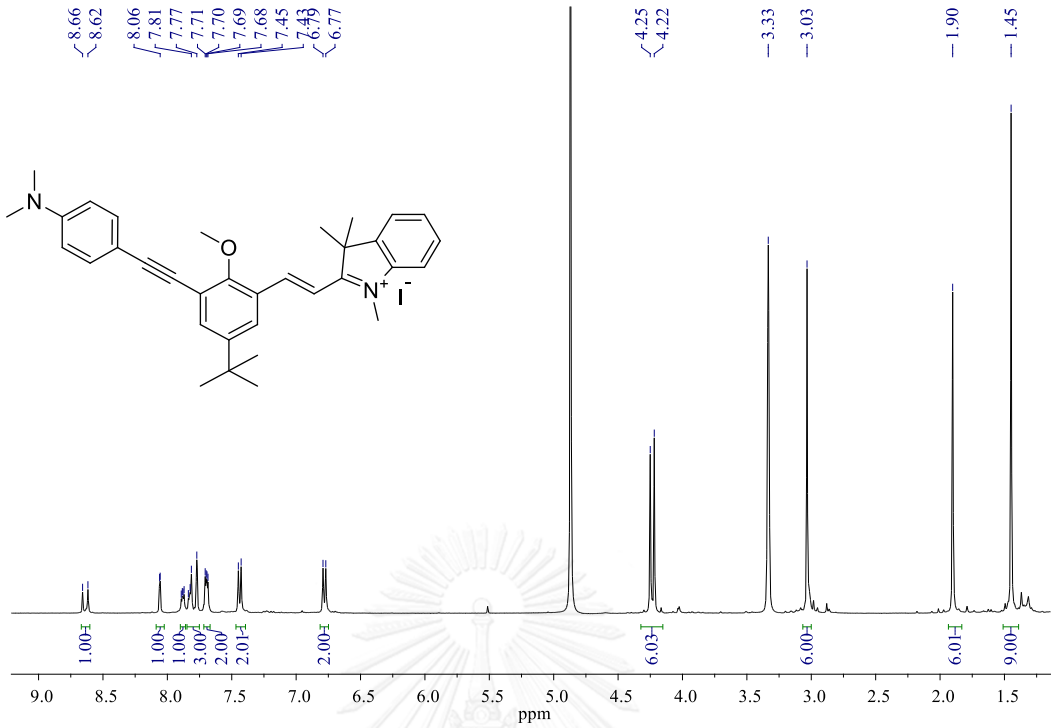

Figure A5 ^{1}H NMR spectrum of compound **3** in CD_3OD.

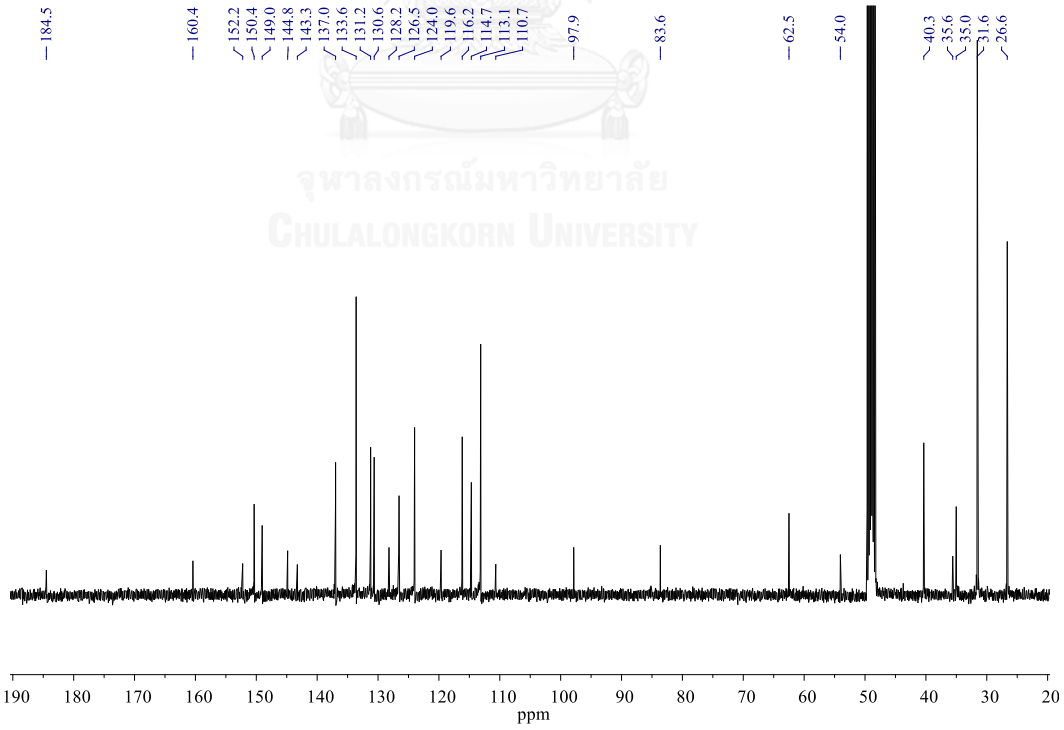

Figure A6 ^{13}C NMR spectrum of compound **3** in CD_3OD.

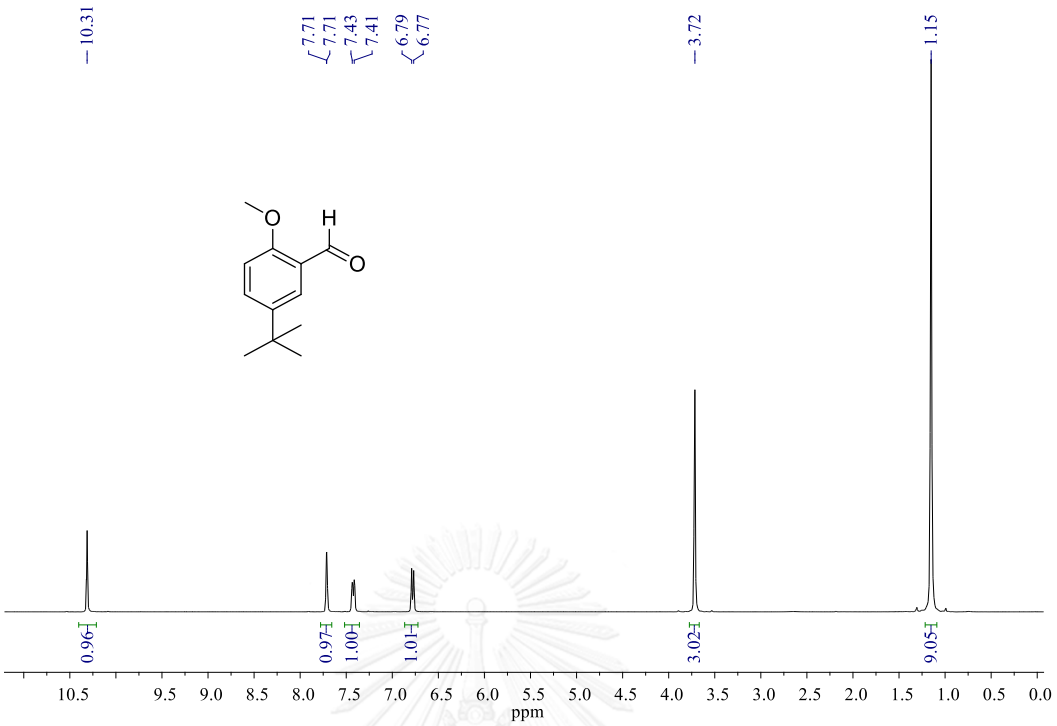

Figure A7 ^{1}H NMR spectrum of compound **4** in $CDCl_3$.

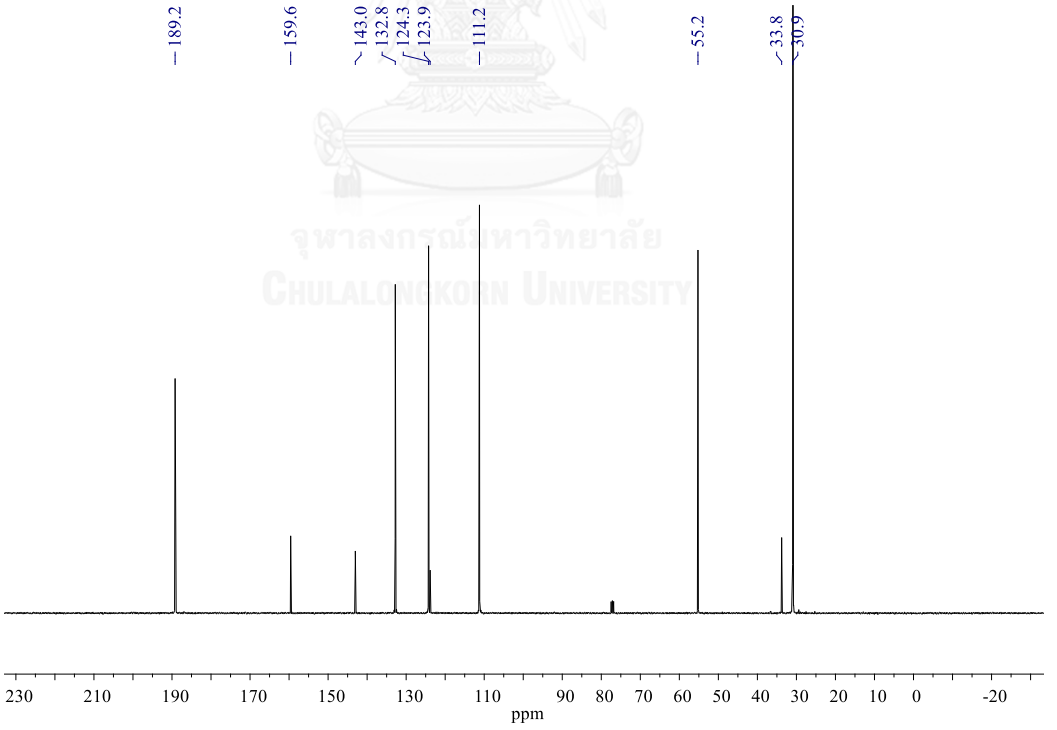

Figure A8 ^{13}C NMR spectrum of compound **4** in $CDCl_3$.

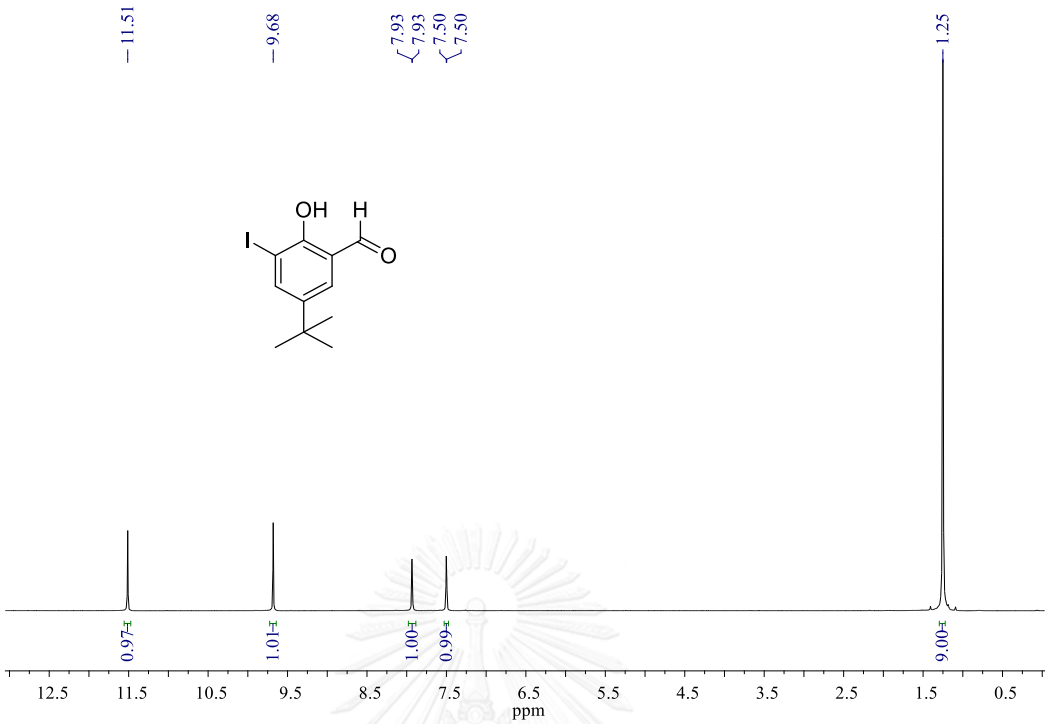

Figure A9 ^{1}H NMR spectrum of compound **5** in $CDCl_3$.

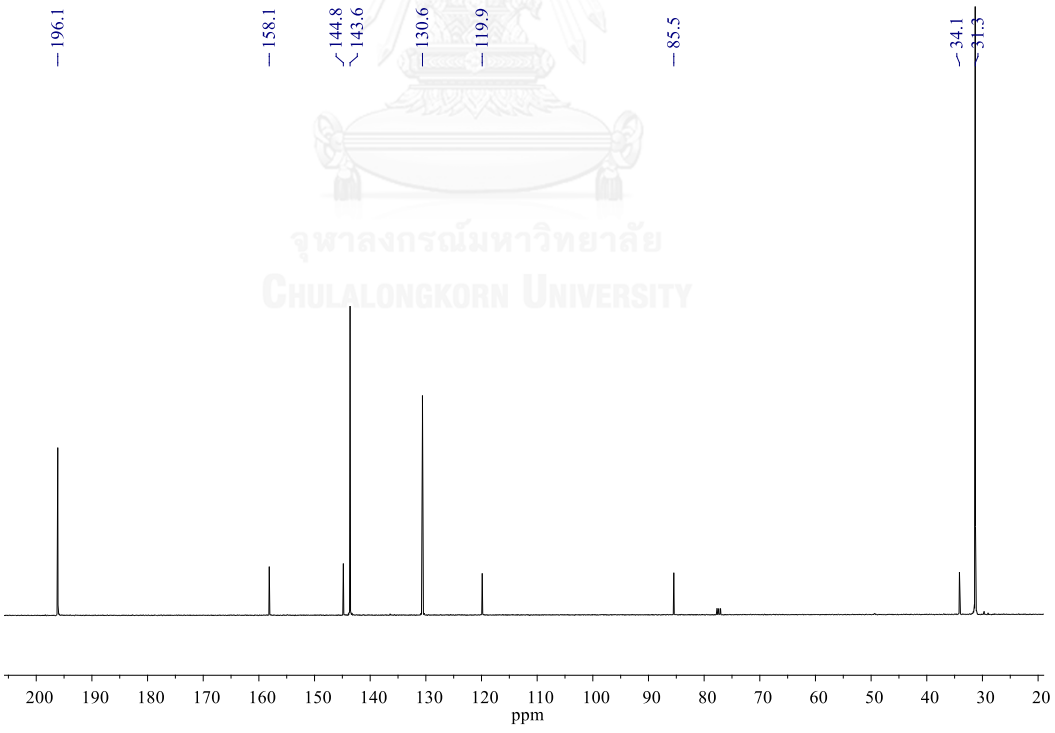

Figure A10 ^{13}C NMR spectrum of compound **5** in $CDCl_3$.

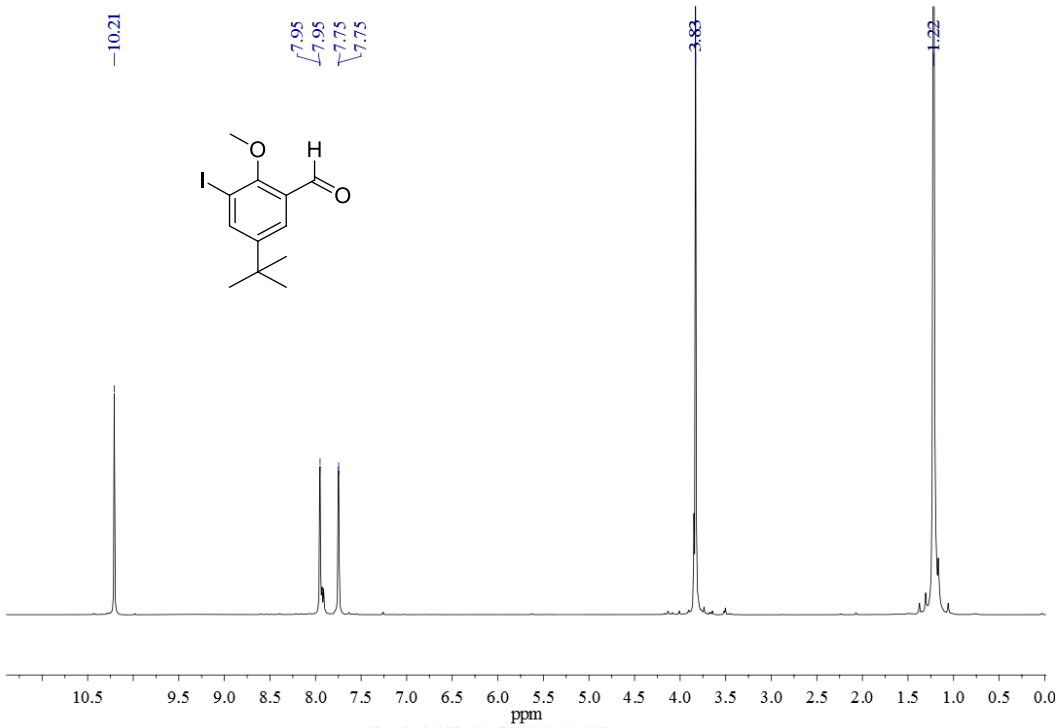

Figure A11 ^{1}H NMR spectrum of compound **6** in $CDCl_3$.

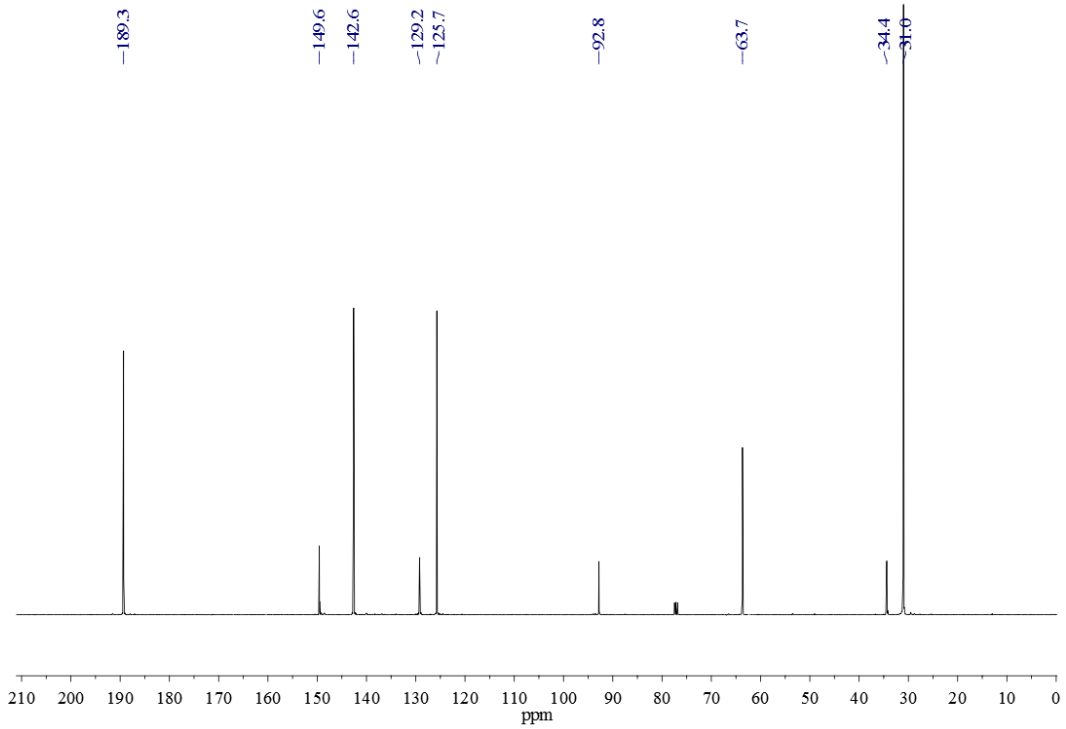

Figure A12 ^{13}C NMR spectrum of compound **6** in $CDCl_3$.

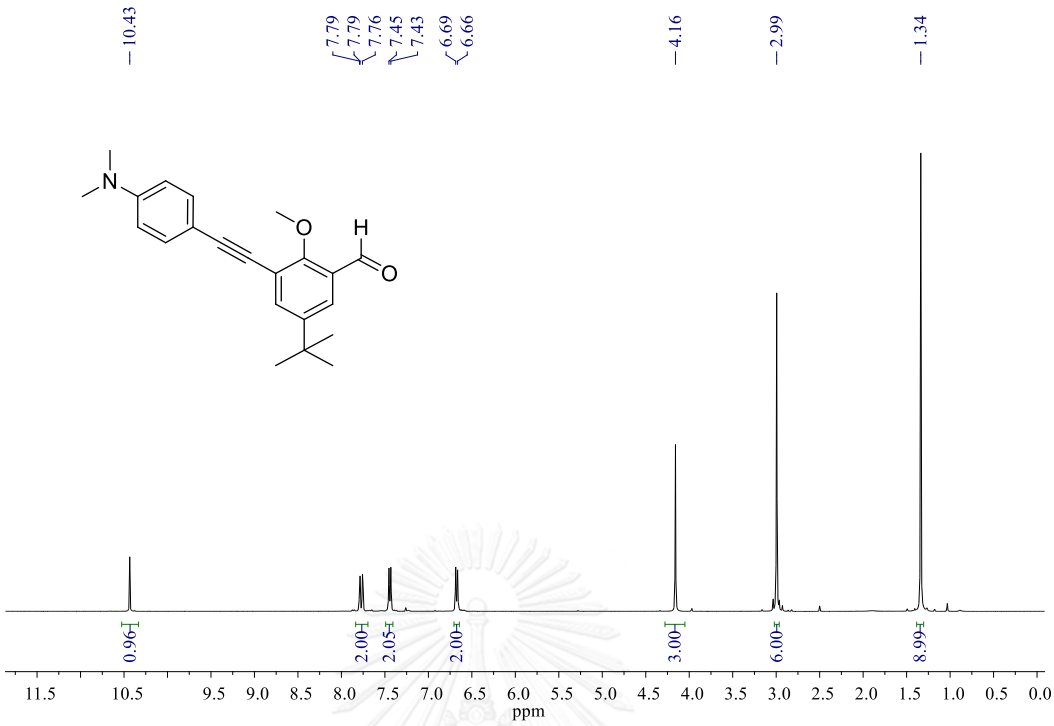

Figure A13 ^{1}H NMR spectrum of compound **7** in $CDCl_3$.

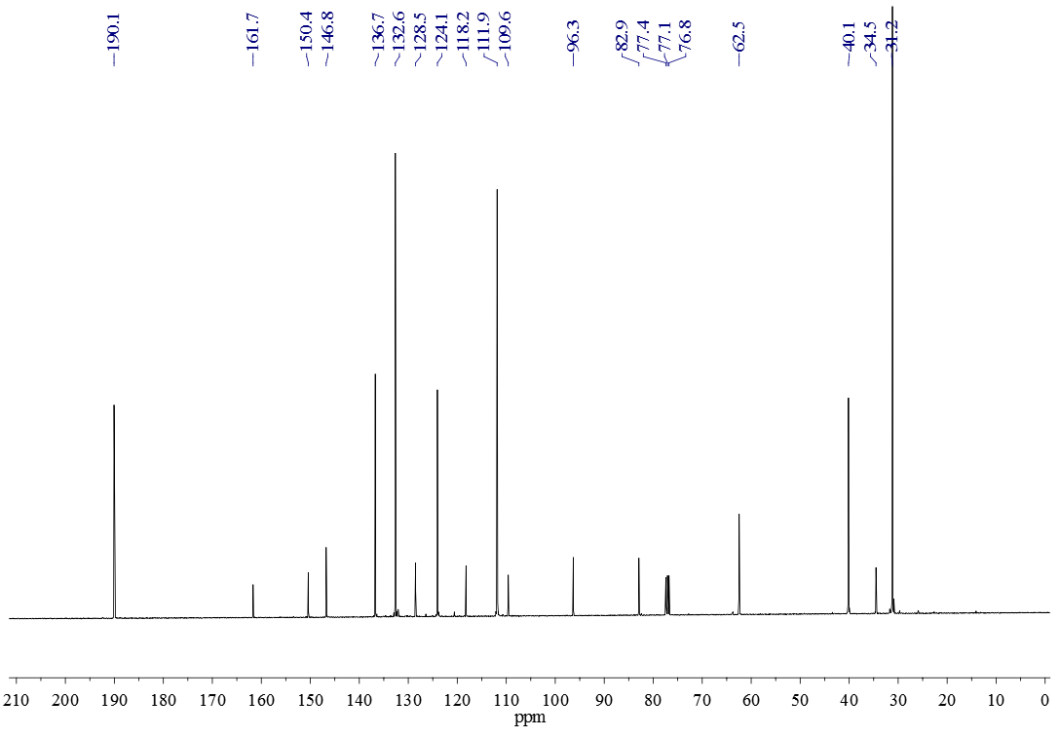

Figure A14 ^{13}C NMR spectrum of compound **7** in $CDCl_3$.

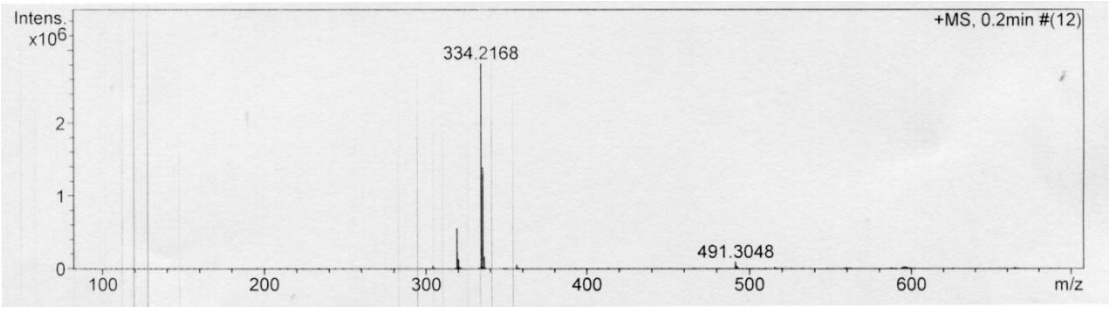

Figure A15 HRMS spectrum of **1b** (m/z calculated for [**1b**+H]$^+$: $C_{23}H_{28}NO^+$ = 334.2165; found 334.2168).

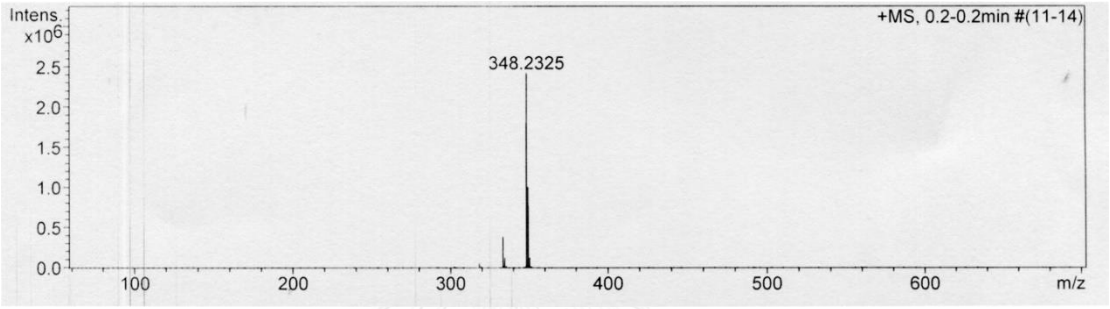

Figure A16 HRMS spectrum of **2** (m/z calculated for **2**: $C_{24}H_{30}NO^+$ = 348.2322; found 348.2325).

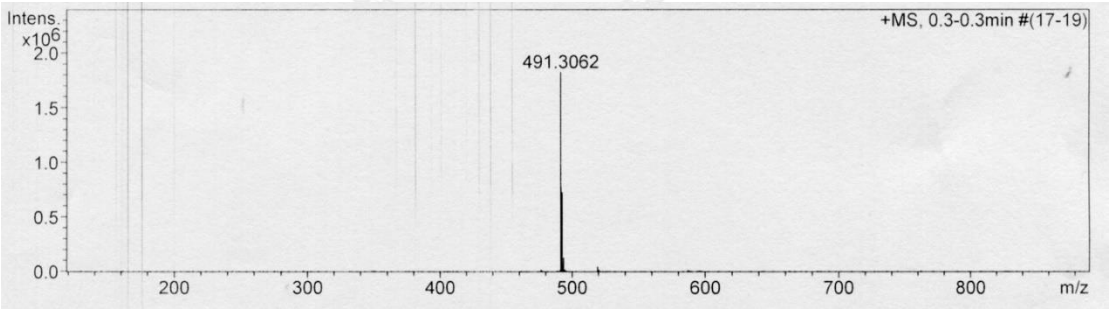

Figure A17 HRMS spectrum of **3** (m/z calculated for **3**: $C_{25}H_{30}N_2O^+$ = 491.3057; found = 491.3062).

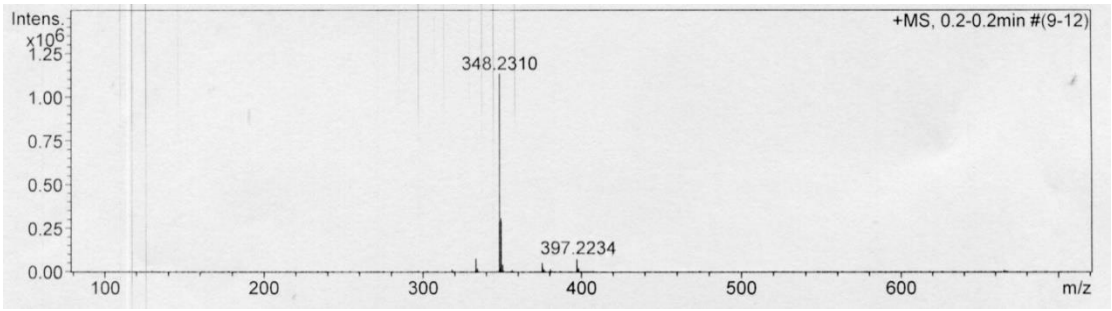

Figure A18 HRMS spectrum of **2**+CN^- (m/z calculated for [**2**+CN+Na]$^+$: $C_{25}H_{30}N_2O$+Na^+ = 397.2250; found 397.2234).

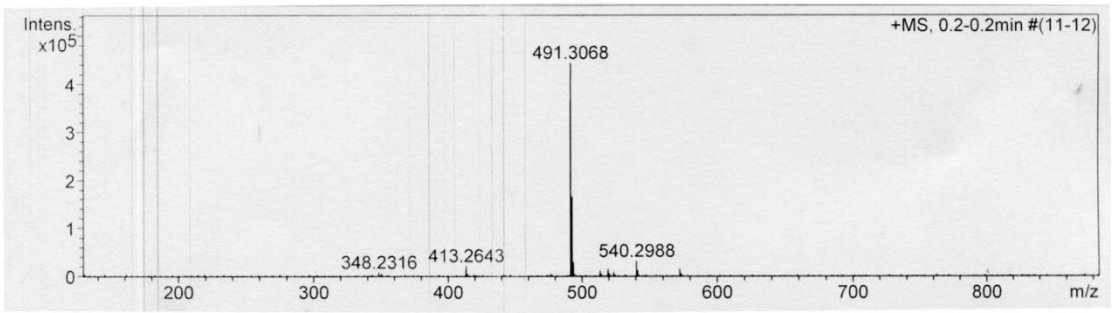

Figure A19 HRMS spectrum of **3**+CN^- (m/z calculated for [**3**+CN+Na]$^+$: $C_{35}H_{39}N_3ONa^+$ = 540.2985; found = 540.2988).

VITA

Mr. Apiwat Promchat was born on October 10, 1991 in Songkhla, Thailand. He graduated with high school degree from Hatyai Wittayalai Somboon Kulkanya School, Songkhla. He graduated with bachelor degree of Science, major of chemistry from Prince of Songkla University in 2012. He has been a graduate student in organic chemistry and become a member of Material Advancement via Proficient Synthesis Group under supervision of Professor Dr. Mongkol Sukwattanasinitt. He has received scholarship from Science Achievement Scholarship of Thailand (SAST) since he was studying in Bachelor degree and he further received a Master Degree in Chemistry from Chulalongkorn University in academic year 2015. His present address is 85 Moo. 2 Soi. 5 Kanjanavanich road, Hatyai, Songkhla, Thailand 90110.